Abstract

A single-stage sounding rocket S-210JA-3 was launched to an altitude of 130 km over Syowa Station, Antarctica, on 22 July 1971, for high time resolution image formings of spatial patterns of auroral X-rays. A pair of NaI (T1) scintillation counters, sensitive to X-ray energies of 4 KeV to 40 KeV, was used at mounting angles of 45° and 135° with the rocket axis. They succeeded in scanning a considerable part of the sky through the composite operation of the spinning and coning motions of the rocket, and recorded X-ray fluxes with a magnitude of the order of 10 times the background X-ray flux. As a result, a sequence of iso-photo maps, taken every 5 seconds, of X-ray fluxes with respect to the azimuthal and elevation angle coordinates was achieved covering different altitudes between 73 km and 131 km.

The forty-four maps thus obtained during the entire flight of 225 seconds demonstrate the fine structures in spatial patterns, and in particular the existence of several points of origin of auroral X-rays and their temporal changes. It will be shown that the gross spatial character of X-rays is well correlated with those of visual aurora seen from the ground and of ultraviolet emissions measured from on board the same rocket. However, detailed comparisons of X-rays with ultraviolet emissions reveal that none of the fine structures of X-ray distributions were detected by means of the ultraviolet detector. The altitude dependence of the X-ray flux will be discussed taking into account temporal and spatial variations of the auroral luminosity.

1. Introduction

Most of the precipitating auroral particles, electrons and protons, by which a variety of auroral phenomena are caused, can not penetrate many layers of the atmosphere. But the bremsstrahlung X-rays radiated from the energetic electrons can reach down deeply to an altitude of about 30 km. Since such auroral X-rays are easily detectable at balloon altitudes, dynamical and morphological studies of them have been performed mostly on the basis of a number of balloon observations. These include simultaneous flights of multiple balloons from different stations (BROWN, 1966; TREFALL, 1970; KREMSER, 1973; TREILHOU, 1974) and conjugate flights with a geo-stationary satellite (PARKS, 1970; BROWN *et al.*, 1968).

However, most of the past balloon experiments were aimed at studies of the time characteristics of total X-ray fluxes integrated over the sky at one station, rather than at studies of the fine structures of individual auroral arcs in the sky, that is, spatial distributions. This situation caused us occasionally to be uncertain and misunderstand direct comparisons of X-ray variations with associated phenomena such as optical line emissions, and geomagnetic field and riometer variations, because the effective fields of view responsible for the respective measurements are somewhat different from each other. Thus, a sort of image forming observation of auroral X-rays is essential and effective for progressive studies of aurora, even if the experiment is limited to a single balloon launched from one station.

On the other hand, rocket observations of auroral X-rays have, in principle, several attractive features superior to balloon observations. They are,

1) X-ray measurements by a rocket are able to cover a very broad field of view because of less atmospheric absorption, in contrast with balloon measurements restricted to a relatively small region around the launching site (IMHOF, 1974).

2) The rocket is usually spin-stabilized with a fast spinning motion of the order of a second or less. Consequently, the directional X-ray telescope

mounted obliquely against the rocket axis can perform efficiently the sky survey, although the region of survey is limited by the solid angle of the detector and also by the precession angle of the rocket, if any. Thus it may result in a number of image patterns of X-rays with appreciably high time resolution (KODAMA and OGUTI, 1974).

3) The minimum energy of X-rays detectable becomes lower by one order of magnitude than at balloon altitudes. Therefore, a much better signal-to-noise ratio is achieved particularly in the lower energy band, in which auroral X-ray fluxes are usually dominant.

4) Little atmospheric modification is expected of the original energy spectrum and the spatial distribution of the precipitating electrons. It is because both the energy degradation due to the photoelectric absorption and the Compton scattering become lower in the thinner air layer (SELTZER *et al.,* 1973).

5) It is possible to measure directional components of X-rays, upward and downward, as a function of altitude. This gives information about quantitative estimation of the photoionization caused by absorption of bremsstrahlung X-rays in the upper atmosphere (KAMIYAMA, 1966).

6) The above-mentioned features should certainly enhance the validity of direct comparisons with all other auroral phenomena.

Among the various advantages described above, the major point of interest is found in item 2, that is, image formings of auroral X-rays, though these are limited to the vicinity of a rocket launching site. Indeed, a special device for imaging by means of high speed photometric scanning has been adopted in a rocket experiment (ROBERTSON *et al.,* 1974). Also, a similar observation has been made of auroral X-ray spectra against the four quadrant spaces around the rocket (VENKATESAN and ANGER, 1975). Recently, satellite observations were performed with the aim of taking global-scale intensity distribution and energy spectra of the bremsstrahlung produced in the atmosphere (IMHOF *et al.,* 1974).

In fact, however, it is not always easy to correctly fit the rocket trajectory into the most exciting region of auroral luminosity, which frequently displays dynamic, rapid movement. Furthermore, the higher resolving power of the position required for recognition of better refined image patterns of X-rays is generally accompanied by poorer counting statistics and also by a greater possibility of being out of limited and discrete regions of X-ray emissions. Similarily, the higher spinning motion, which is essential not only for the stable flight of rocket but also for better time resolution of the rocket-borne instruments, is incompatible with better statistics in flux.

Considering these circumstances, it seemed, for our first rocket experiment in Antarctica, more desirable to be sure to catch the X-ray source during the

flight wherever the aurora appeared, rather than to expect better discrimination of energy or source locations. In addition, we had to take into account the flight characteristics of the rocket used in the present experiment.

Our S-210JA type rocket is small and single-staged so that its flight aspect is not always stable and often subject to a considerable degree of precession motion. Such precession motion is, however, rather favorable for the all-sky scannings we want, because the scanning region determined by the solid angle of the instruments is extended further by the possible range of the precession angle. Using the maximum height of arrival of the rocket in connection with the aforementioned item 5, a pair of identical detectors, mounted forwards and backwards, were set so as to detect, with a degree of certainty of 80% or more, all X-ray fluxes coming from specified auroral arcs, even if they appeared in anypart of the 4π hemisphere.

The S-210JA-3 rocket was launched from Syowa Station (69°00′S, 39°35′E), Antarctica, on 22 July 1971, as part of the 12th Japanese Antarctic Research Expedition program, and carried a pair of NaI scintillation counters to the maximum height of 131.4 km. These counters succeeded in recording in flight the remarkable enhancement of auroral X-ray fluxes, which amounted to the order of 10 times the background flux due to cosmic rays. As a result, a sequence of iso-photo maps of X-ray fluxes was obtained from a relatively broader field of scanning owing to an unexpectedly large precession motion of which the half angle was close to $\pi/2$. Descriptions of the rocket-borne instruments and the gross feature of auroral activity before and after the rocket was fired are given in Sections 2 and 3, respectively. In Section 4 the atmospheric absorptions of the auroral X-rays are noted. Modulation effects of spinning and precession motions of the rocket on X-rays are described in Section 5 and spatial distributions of X-rays deduced from them are given in Section 6. An ultraviolet detector was on board the same rocket. Results from the simultaneous observations taken by it with X-ray measurements are compared and discussed in Section 7. Discussions are contained in Section 8 of comparisons of the X-ray patterns with other related auroral phenomena. Finally, the physical meanings of the resultant spatial patterns of X-rays are discussed in Section 9, with some uncertainties included there.

2. Instrumentation

For the aim of tracing spatial distributions of auroral X-rays using a rocket, it is desirable to try sky surveys with position and time resolutions as fine as possible. In practice, this may be subject to both the actual strengths of detectable X-rays and such instrumental limitations as telemeter response and available geometrical capacity. Hence, it is not always easy to decide the optimum design of instruments so as to satisfy all arbitrarily variable parameters. It is, however, expected that the usage of at least two identical detectors pointed in opposite directions could improve the power of time resolution and the reliability of experimental data.

The payload used in the present rocket experiment consists of a pair of NaI (T1) crystals (25.4 mmϕ $\times$ 2 mm thickness), each of which was viewed by an RCA 2060 photomultiplier tube. They were mounted at inclined angles of 45° (forward) and 135° (backward) with the rocket axis. An Sn collimator attached to the crystal was of conventional grid type, having a solid angle of 19°40′ (26°50′ in diagonal). From considerations of the thermal noise level of the photomultiplier tube and of the background X-rays due to cosmic rays, the range for measuring the energy of the X-rays was set between 4 KeV and 40 KeV. The expected maximum value of omni-directional fluxes of auroral X-rays at balloon altitudes over Syowa Station given by KODAMA *et al.* (1972) led us to the determination of the dynamical range of allowable counting rates of the instruments. Thus it was designed to be zero to 10^5 per second in accordance with a two-stage step counter system, in which the telemeter response available is less than 220 Hz. A general outline of the payload and the block diagram of its electric part are shown in Figs. 1 and 2. Also given, in Fig. 3, is a small sample of the pen-writing records actually obtained by the step counter system.

Prior to the flight, apparent sensitivities of the above two counters (hereafter termed F- and B-counters for convenience) to different X-ray energies were calibrated using ^{55}Fe and ^{109}Cd radioactive sources. The results showed a little difference between both the counters. Namely, the energy sensitivity

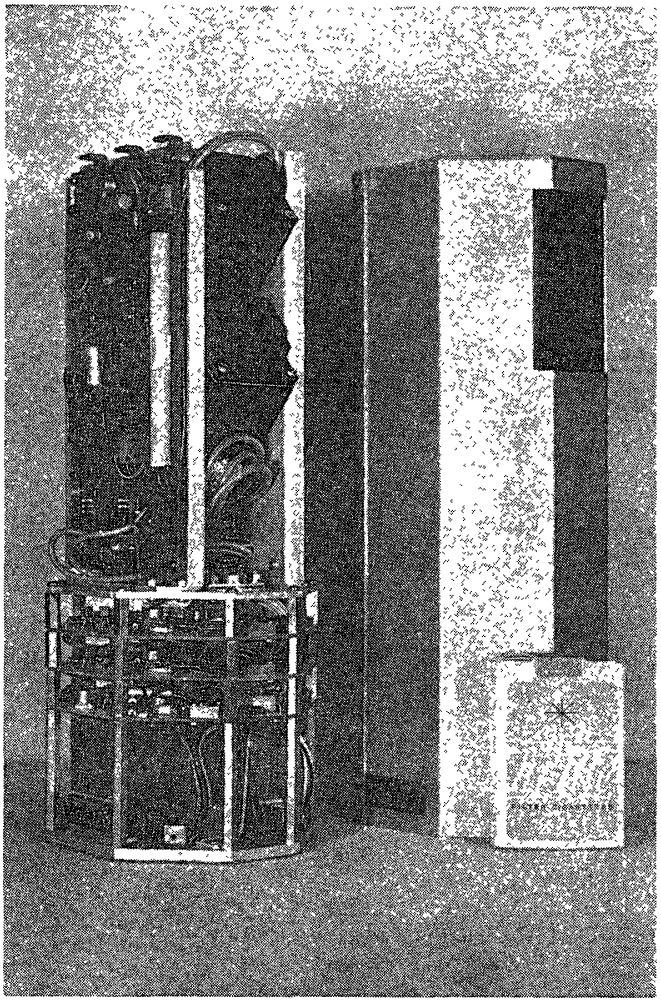

Fig. 1. A rocket-borne instrument measuring auroral X-rays.

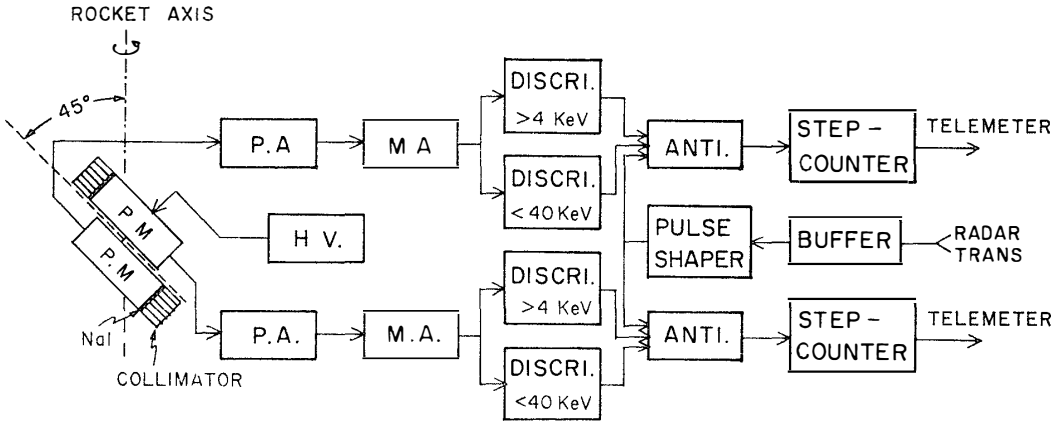

Fig. 2. A block diagram of the electronic part of the rocket-borne X-ray instrument.

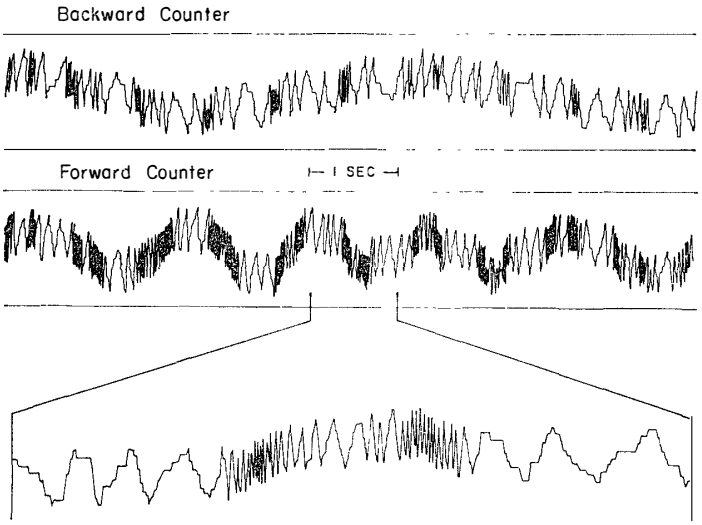

Fig. 3. A small reproduction of pen-writing records actually obtained by means of the two X-ray counters, forward and backward, during the rocket flight. A two-stage counting system was adopted: the first stage registers 2^4 counts from the counter and the second stage includes 2^6 peaks on top of the first one.

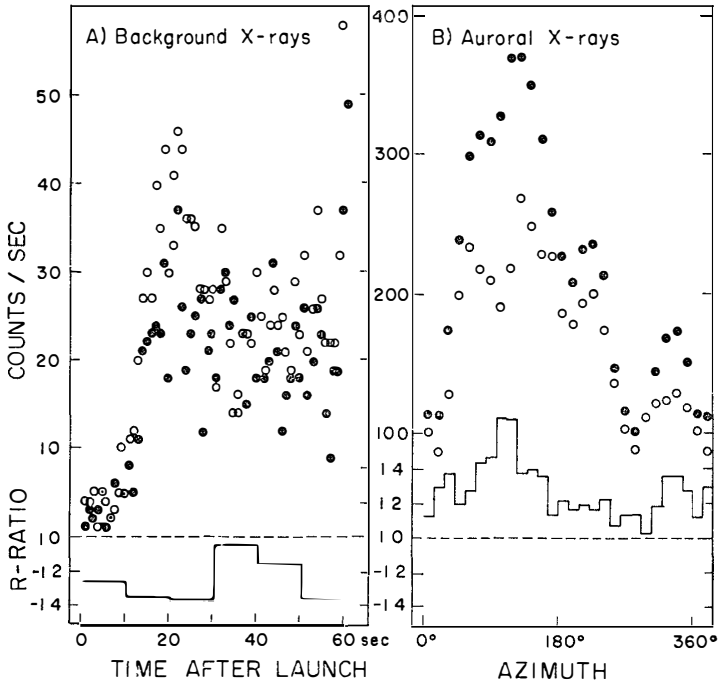

Fig. 4. Counting rate responses of the forward and backward X-ray counters on (A) background X-rays during the ascent and (B) auroral X-rays during a selected precession period. Counting rates from both the counters are indicated by solid and open circles, respectively. In the lower portion is given the count ratio R defined by $2(C_F-C_B)/(C_F+C_B)$, where C_F and C_B are counts from the forward and backward counters respectively.

of the B-counter in relation to the F-counter was 1.064 for ^{55}Fe (~6.4 KeV), and 1.173 for ^{109}Cd (~22 KeV). This seems to be due to the different characteristics of the photomultipliers, the non-symmetrical arrangement of materials around each of the counters and some other factors.

Actual evidence suggesting such sensitivity differences between the two counters were given by both the altitude dependence of the background X-rays and the azimuthal dependence of the auroral X-rays. Fig. 4 shows the intensity-time profiles of the background and auroral X-rays recorded during the ascending period and a selected precession period of the rocket, respectively. Also shown in the lower portion of the diagram are the sensitivity differences defined by the quantity $R=2(C_F - C_B)/(C_F + C_B)$, where C_F and C_B are the counting rates from the forward and backward counters respectively. It should be noted that R is negative for the background X-rays while positive for the auroral X-rays. This means that the F-counter is more sensitive to relatively lower photon energies while the B-counter is more sensitive to higher energies; this being consistent with the above-mentioned pre-calibration results.

3. Rocket Flight and Associated Auroral Activity

A single-stage sounding rocket S-210JA-3 was launched from Syowa Station (69°00′S, 39°35′E), Antarctica, at $00^h52^m01^s$ LT* on 22 July 1971 and 173 seconds later it reached a maximum height of 131.4 km. The rocket altitude *versus* time curve is shown in Fig. 5. The nose cone cap of the rocket was removed 60 seconds after firing (at ~ 70 km in altitude) and thereafter auroral X-rays were recorded continuously until re-entry into the atmosphere. The maximum counting rates of X-rays were obtained at 280 seconds after launch, at which time they showed about 40 and 26 times the intensity of the background X-rays for the F- and B-counters, respectively.

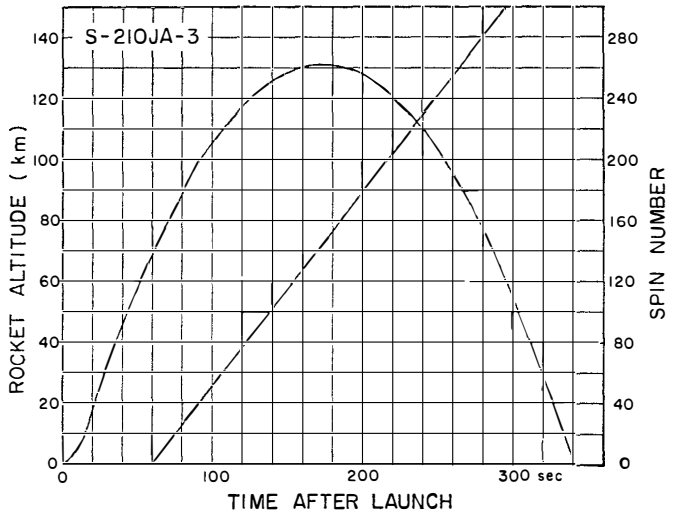

Fig. 5. The rocket altitude versus time after launch is given by a parabolic curve. Serial spinning numbers, for the time after the rocket nose cone was removed 60 sec after launch, are also indicated by a straight line.

* 2152 UT approximately equals to the magnetic local time at Syowa Station.

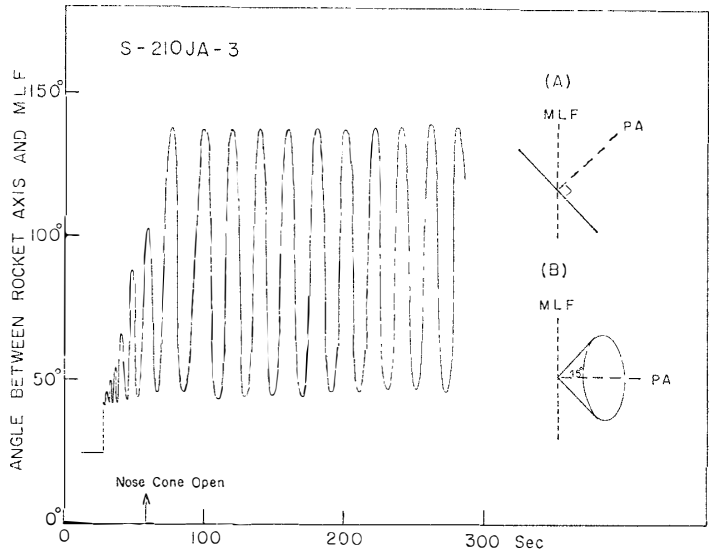

Fig. 6. Time variations of the rocket attitude are represented by the angle between the spinning axis and the geomagnetic line of force. The right-hand side diagram shows the two allowable cases of the precession axis with respect to the m.l.f. Only case (A) was realized (see text).

The flight attitude of the rocket was estimated from the records of a geomagnetic aspect sensor on board. Fig. 6 shows the time variation of the angle between the rocket axis and the geomagnetic field line during the entire flight. It is obvious that the flight attitude was not stable but varied widely in making the inclination from 43° to 137° as measured from the geomagnetic field line during the greater part of the flight. This fact means that the preces-

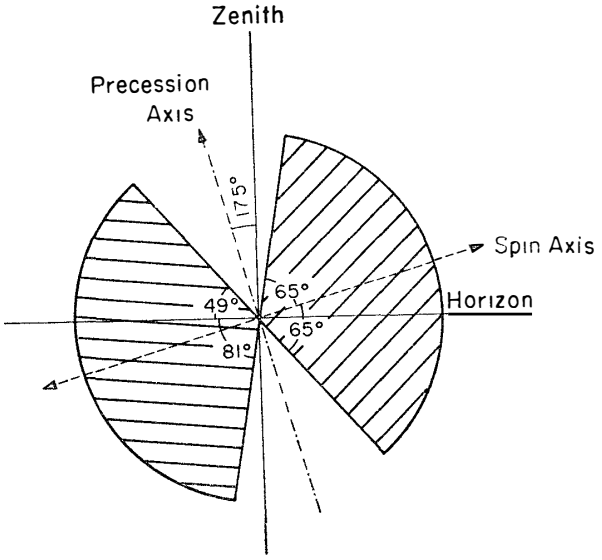

Fig. 7. Projections of the main fields of view of the X-ray counters on a plane including both the zenith and the rocket's horizon. Each of two fan-shaped patterns, rotating in fact around the precession axis, corresponds to either the forward or backward counter alternatively.

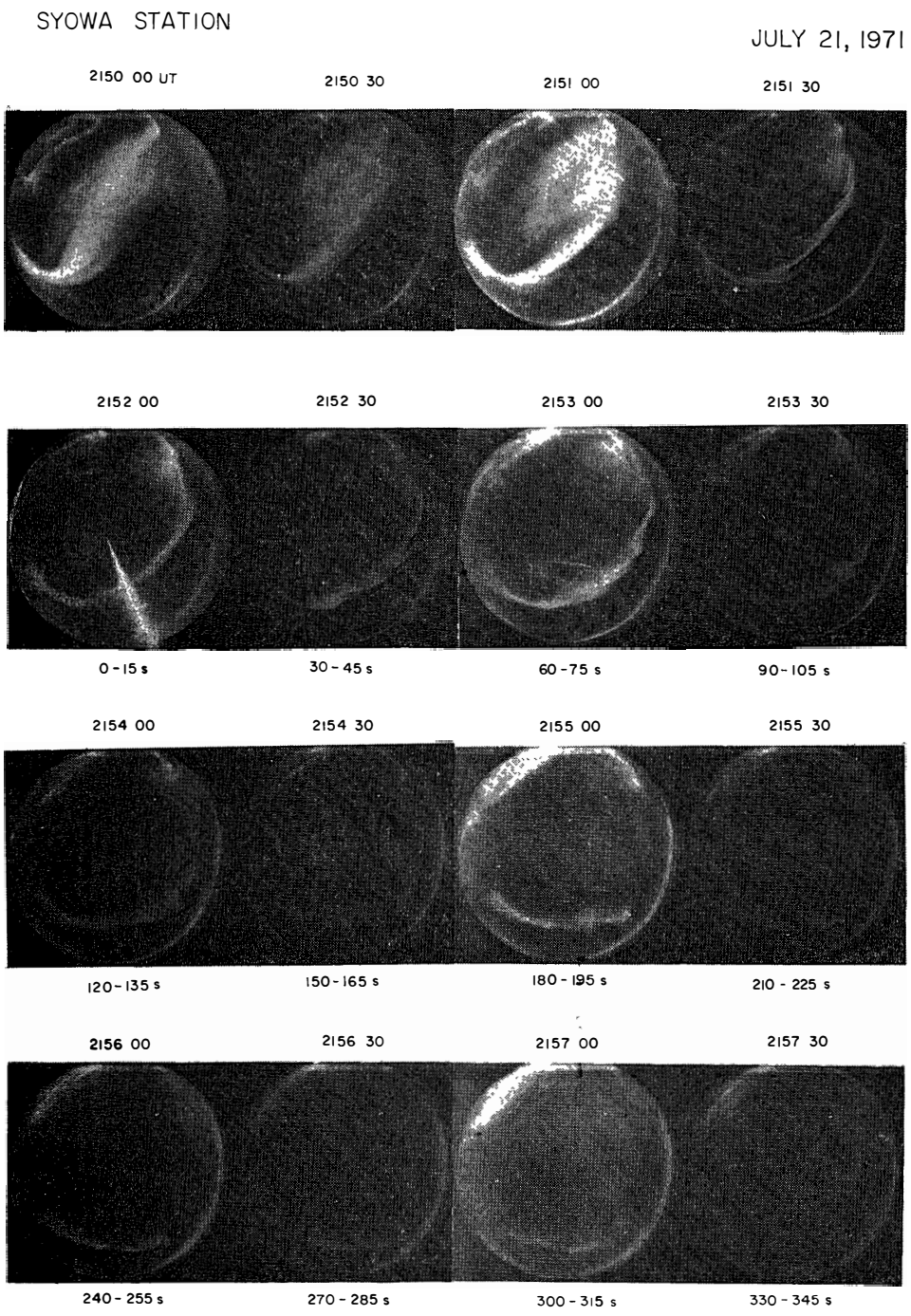

Fig. 8. A sequence of all-sky camera photographs taken every 30 sec at Syowa Station, where the exposure time was set alternatively at 15 sec or 30 sec. The bright stream appearing at 2152 UT displays the rocket trajectory. The elapsed time after launch is also indicated below each photo. The top side of each photograph points to the geomagnetic east and the right-hand side to the north.

sion angle of the rocket is either $43° + 137° = 180°$ or $137° - 43° = 94°$. However, from the comprehensive survey of auroral X-ray data, of which descriptions will be given in Section 5, it is concluded that half a conical angle of the precession equals the former, or, 90°. In other words, the present rocket flew in rotating with a precession period of 20.47 seconds, like a boomerang inclined at about 17.5° from the horizon line. In addition, a rocket spinning frequency of 1.27 Hz was determined from the same X-ray data. Consequently, the fields of view of the two X-ray counters fairly well overlapped with each other, as illustrated in Fig. 7. This made it possible to trace auroral X-ray patterns with double accuracy precision.

A general view of the auroral activity, which appeared during the present experiment, can be seen from the all-sky camera photographs taken simultaneously at Syowa Station. Fig. 8 shows examples of these photographs taken every 30 seconds with an alternative exposure time of 15 or 30 seconds. It is evident from the series of photographs that the discrete type of auroral arcs, whose peak luminosity was about 5 KR (for 4278 Å), where in the fading phase and moving rapidly from south-east to north-west. When the rocket was fired, the brightest arc was already far from the overhead point and located near the horizon. This situation was rather favorable for the present particular view-fields of the detectors aimed predominantly in the horizontal direction, so that most of the X-rays emitted from the auroral arcs could be detected well and efficiently.

4. Atmospheric Attenuation of Auroral X-Rays

In Fig. 9 are shown the entire time profiles of auroral X-ray intensities measured by the two X-ray counters F and B, where the 1-spin counting rates are plotted to form the gross feature of variations free from the spinning modulation. As clearly seen from the figure, the periodic variations due to the precession motion after the removal of the nose cone are quite dominant and yet they are exactly out of phase between a pair of recordings because of the opposite mounting of the detectors in the azimuth. Thus, a simple summation of both the counting rates exhibits the intensiyt-time profile without precession modulation but with some altitude dependence.

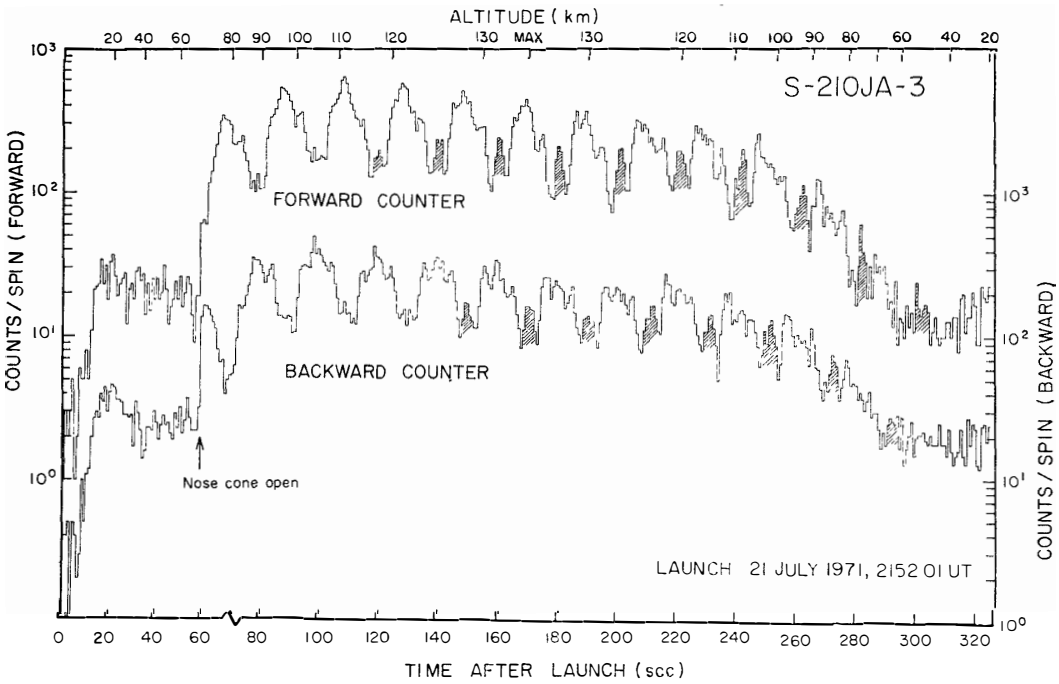

Fig. 9. The entire time profiles of auroral X-ray intensities measured by the two identical counters, forward and backward, from launch to telemeter off, where 1-spin counting rates are plotted to eliminate the spinning modulation.

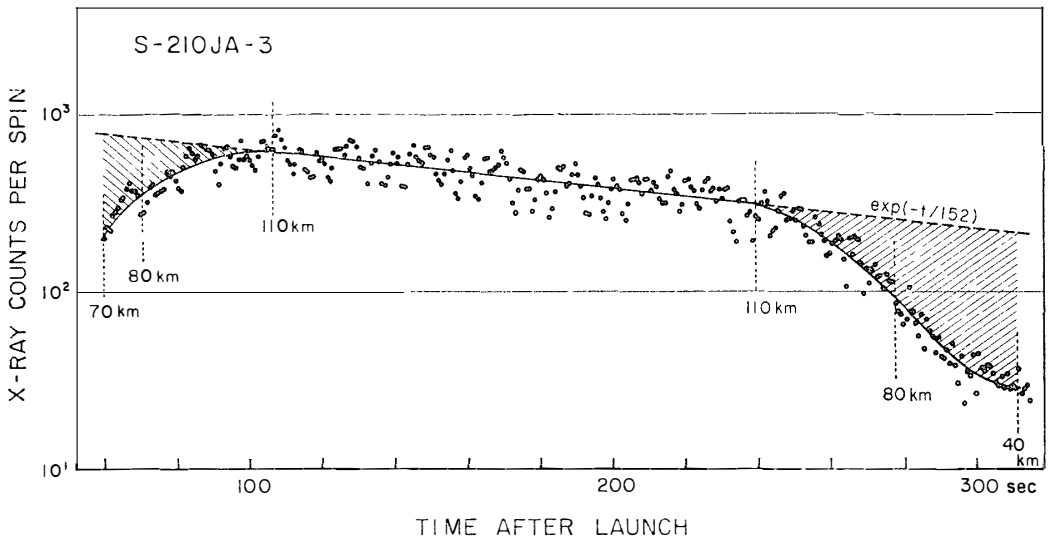

Fig. 10. Time variations of summations of pairs of counts from the two counters, where 1-spin counts are plotted with a straight line approximately fitted to them. The intensity depressions from the straight line, indicated by the shaded area, are due to the atmospheric absorption of X-rays.

Since time variations of such composite intensities at heights of 110 km or more can approximately be fitted by an exponential curve with a coefficient of -152 counts/sec, as shown in Fig. 10, it is considered that this downward grade of intensity is not due to the altitude dependence of X-rays but is accompanied

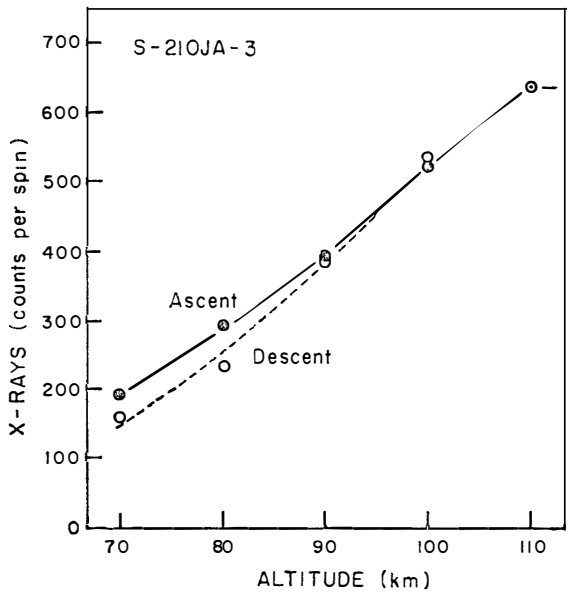

Fig. 11. The altitude dependences of auroral X-ray intensities measured in ascent and descent of the rocket respectively.

by the gradual lowering of auroral activity as evident from Fig. 8. Therefore, assuming the extrapolation of the above straight line toward lower regions of altitudes less than 110 km, the difference between individual observation points and the extrapolated line, as shaded in Fig. 10, should give the apparent altitude dependence of auroral X-rays. Thus the derived altitude dependence in the two phases of ascent and descent are shown in Fig. 11. Both of the curves are fairly consistent with each other, suggesting the satisfactory operation of the instruments during the entire flight. There appears, however, a little discrepancy between them in accordance with a lowering of altitude. This may be attributed to the difference in the atmospheric absorption of X-rays, a description of which follows.

During the period when the present rocket experiment was carried out, bright auroral arcs moved fairly rapidly from SE to NW, as seen in Fig. 8. Such a displacement largely altered the mutual distance between the rocket and the brightest sources, from which auroral X-rays were predominant, from time to time. Considering the two different moments corresponding to the altitude of 70 km on the ways of ascent and descent, the rocket-source distance in the descending phase elongated to about four times that in the ascending phase, when setting the average height of the source at 110 km. Then the altitude dependence of Fig. 11 can be transformed into a relationship with the atmospheric

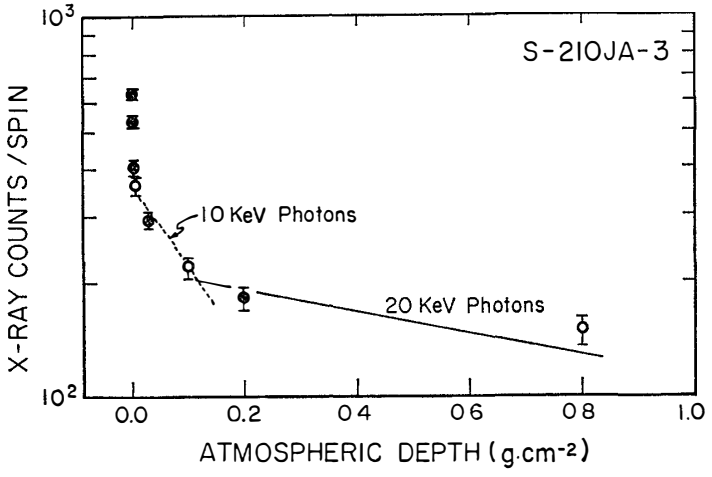

Fig. 12. Auroral X-ray intensities as a function of atmospheric depth, where solid and hollow circles are for ascent and descent of the rocket respectively. Two straight lines, broken and solid, represent the altitude dependences of X-rays drawn on the basis of the absorption coefficients of 10 KeV and 20 KeV photons in air, respectively.

depth, as shown in Fig. 12. In this case, there is no more discrepancy between the two different phases. Therefore, the altitude effect observed in heights of less than 90 km is attributed to the atmospheric attenuation of X-rays due to photoelectric absorption and Compton scattering. In other words, no atmospheric effect on X-rays is found at heights over 90 km.

There still remains, however, a sharp intensity increase in depths close to zero. This may be probably caused by a possible temporal change in the geometrical association between the viewfield of the detector and the source location as the rocket approaches very near to the X-ray sources. Since the X-ray detector generally records all of the fluxes integrated along its line of sight, it gives the maximum X-ray intensity when the detector is located in the same level as the source layer. However, we have no information about the vertical distribution of the source layers, so that the above interpretation is not beyond qualitative imagination.

5. Spinning and Precession Modulations of Auroral X-Rays

Prior to the launch, the spinning motion of the rocket was controlled to give a spinning period of about a second. So a certain degree of spinning modulation of auroral X-rays was expected in advance. Whereas we had expected little precession motion of the rocket, but distinct precession modulations were in fact observed as already seen in Fig. 9.

First, in order to estimate exactly the spinning period by using the obtained X-ray data, 50 msec-counts of the data were read out. An example is illustrated in Fig. 13. Since double peaks of X-ray counts appeared periodically in association with the spinning period, one can derive the spinning period from the time intervals between the adjacent double peaks. Since there occurred 18 repetitions of the double peak patterns during the time interval of 13.4 sec from +100.6 sec to +114.0 sec after launch, we obtain a spinning period of 13.4 sec/17=0.788

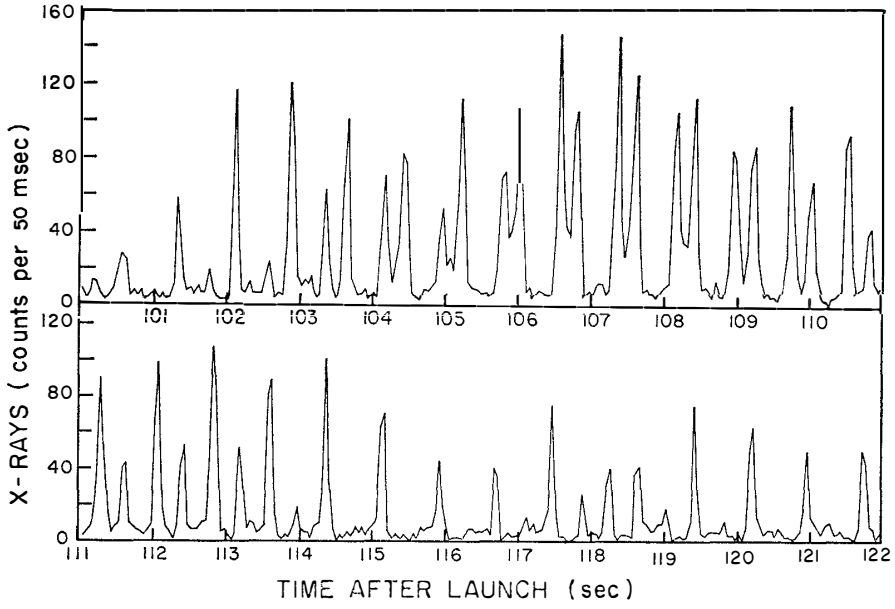

Fig. 13. A part of the time profiles of auroral X-ray intensities, where 50-msec counts from the forward counter are plotted.

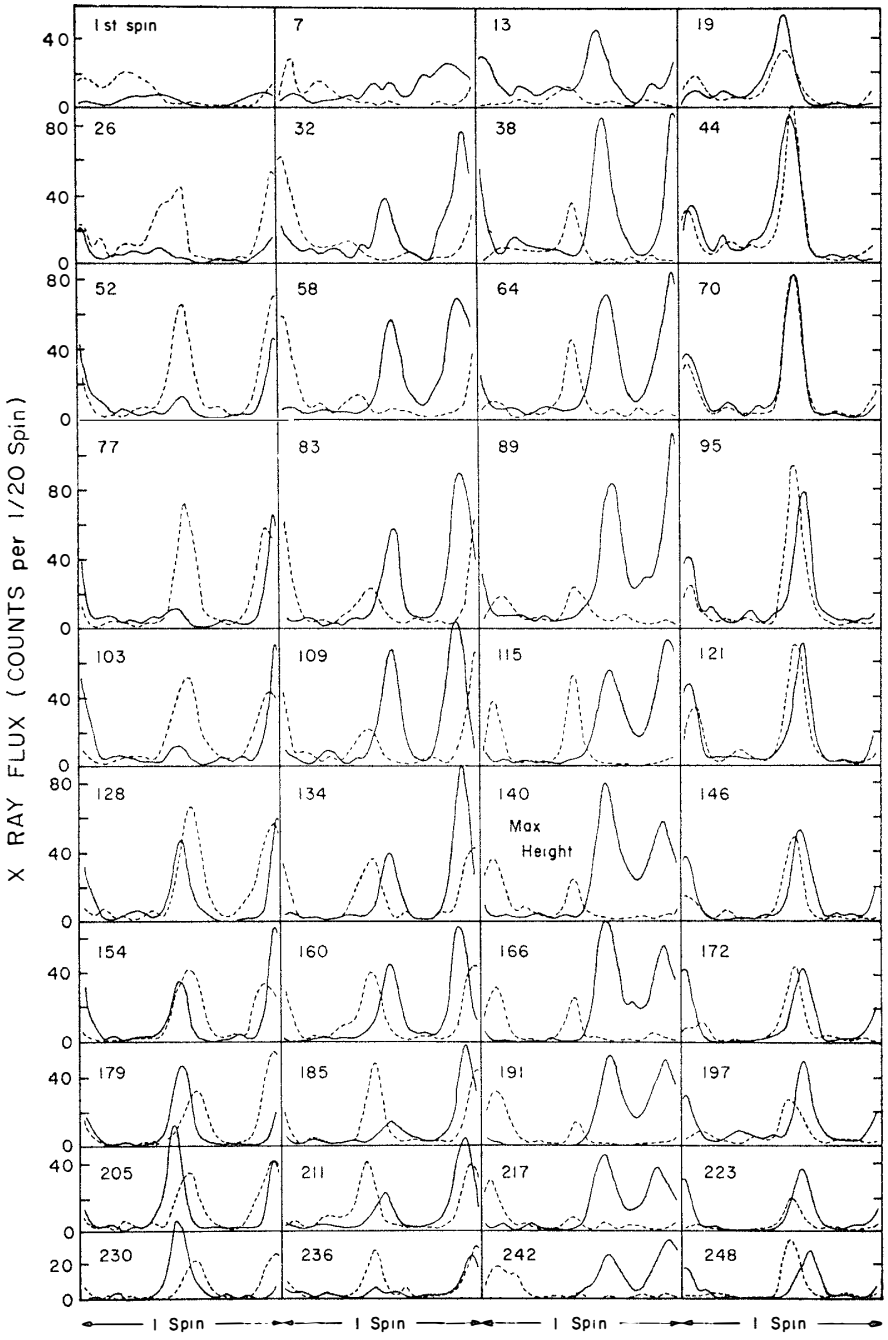

Fig. 14. Typical examples of the spinning and precession modulations of auroral X-ray intensities. Solid and broken curves are for the forward and backward counters, respectively. The numerical figure attached to each panel is a serial spin number as shown in Fig. 5. Note that a similar pattern is repeated every 26 spins.

sec, or, a frequency of 1.27 Hz. Serial numbers of the spinning periods thus derived after the removal of the nose cone are indicated in Fig. 5. It should be noted that the double peak pattern was modulated into a train of single peaks in the latter part of Fig. 13. This directly reveals the temporal modulation of the X-ray source intensity, which will be described in Section 9.

To examine whether or not the above determined spinning period stays constant throughout the entire flight, one twentieth spin counts were read out and selected examples of them were plotted every spin cycle in Fig. 14. The locations of one or two distinct peaks within a spinning period are found to be nearly the same for each series of the different quadrant directions around the rocket. Hence, it is concluded that the spinning motion stayed constant until the end of flight.

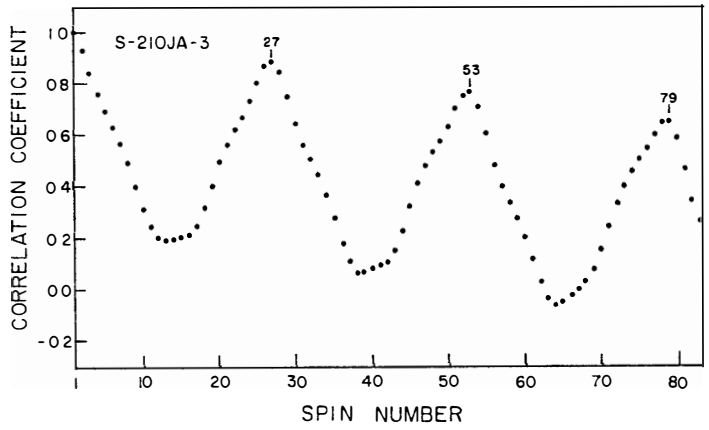

Fig. 15. The auto-correlation diagram of 1-spin counts of auroral X-rays against the spin lag number. Since 2nd, 3rd and 4th peaks appeared at No. 27, No. 53 and No. 79 spins respectively, the precession period is found to contain 26 spins.

Next, the precession period was determined from the auto-correlation analysis using the 1-spin counting rate data. Fig. 15 shows the correlation coefficients as a function of the spin lag number. It is obvious from the figure that the periodic appearance of maxima is seen exactly every 26 spins. It is, therefore, concluded that the precession period is given by 26/1.27 Hz = 20.47 sec. This is in very good agreement with the value deduced from the geomagnetic aspect data of Fig. 6.

As already mentioned, the periodic intensity variations of auroral X-rays which appear in Fig. 9 were those caused by both the precession motion and the non-uniform azimuthal distribution of the active auroral arcs from which X-rays were emitted. There are double intensity enhancements within a pre-

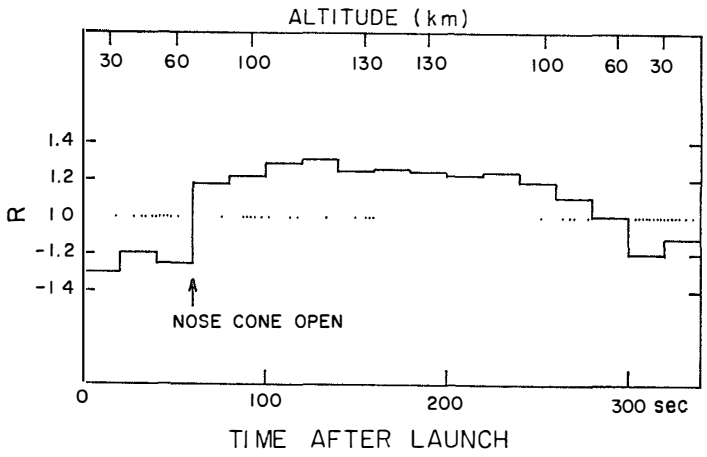

Fig. 16. Time variations of the ratio R representing the sensitivity difference between the two X-ray counters. Note that a positive value is found for auroral X-rays whereas the values for the background X-rays which are dominant in lower altitudes are negative.

cession period of 20.47 sec, a larger one and another smaller one shaded in Fig. 9. Averaging each of them over eleven precessions to see the fine structure of the larger one, the existence of at least four X-ray sources, spaced by 69°, 97°, 111° and 83° in azimuthal angle from each other, were recognized as seen from Fig. 4B. This means that there was a non-uniform distribution of X-ray sources in space during the flight time.

As described in Section 2, Fig. 4 shows the difference in the absolute sensitivity between the two X-ray counters, where the difference was represented by the quantity R. Here, the R-values are calculated every precession and are shown in Fig. 16. These are clearly opposite values between the background X-rays and the auroral X-rays. Since they also are almost fixed around a value of 1.2 at altitudes over 70 km, the azimuthal dependence of R found in Fig. 4B suggests that the energy spectrum may not be always similar from source to source, that is, a larger intensity source is accompanied by a softer energy spectrum.

6. Spatital Distributions of Auroral X-Rays and Their Temporal Variations

As mentioned earlier, the present rocket-borne X-ray counters were accompanied by 26 encircling surveys making an $\sim 90°$ cone of acceptance around the rocket axis during a precession period of 20.47 sec. Consequently, one-fourth of a precession motion is good enough to accomplish one azimuthal round survey, because we have two identical counters pointing in opposite directions from each other. From the time of nose cone removal until telemeter off, 13 precession motions in total were confirmed from geomagnetic aspect and X-ray records. When the X-ray records are read out every 1/20 spinning period, we can obtain from each of the counters $20 \times 26 \times 13 = 6760$ data, in which the maximum counting rates were 130 and 84 for the F- and B-counters, respectively.

In order to compose iso-photo maps giving the spatial distribution of the X-ray sources on the basis of the above sequential data of counting rates, the most essential point is how to find the correct direction of the instantaneous field of view of each counter as well as the correct attitude of the rocket. To do this, we may start from the understanding that half a conical angle of the precession is either $\sim 47°$ or $\sim 90°$ as mentioned in Section 3.

Since the auroral arc which was expected to be the source of X-rays was located fairly distant from the rocket, the detector on board should see the X-ray sources near its horizon. The spinning motion of the rocket should make the viewfield of both counters spin with half a conical angle of 45°. These conditions suggest that if half a conical angle of the precession is $\sim 47°$, neither counter should catch any X-ray sources within its field of view during spin scanning in a precession period, since the magnetic dip is 66° at Syowa Station and the sources are located near the rocket horizon. However, the actual records indicate that each spin-scanning covers the source region twice or at least once, as seen in Fig. 13. It is, therefore, concluded that the half a conical angle was not $\sim 47°$ but $\sim 90°$, and further that the precession axis was quite near vertical.

Thus we can readily expect that the X-ray sources are aligned along a

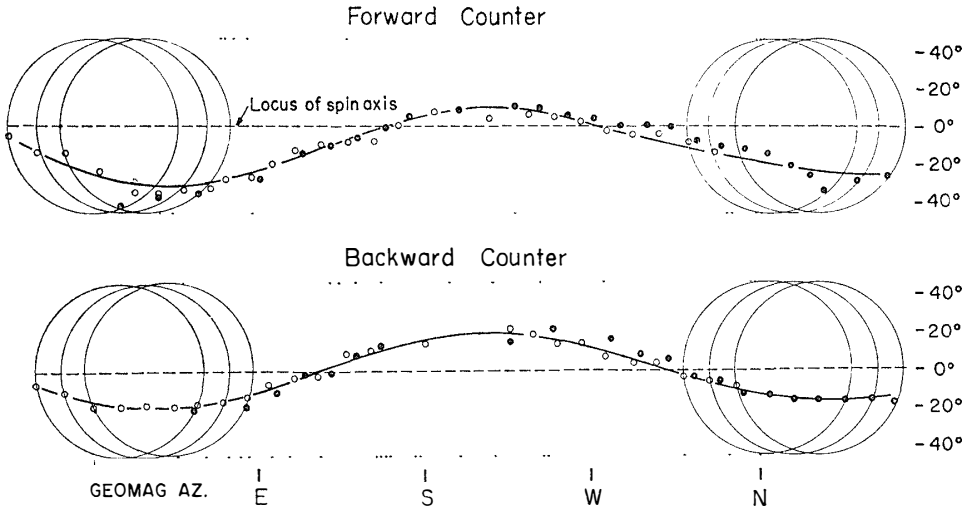

Fig. 17. A train of the two peaks of auroral X-ray intensities which appear once every spinning motion during a precession, with respect to the coordinates of geomagnetic azimuth and the elevation angle measured from the rocket horizon. Small open and solid circles correspond to the preceding and the following halves of a large circle of spin, respectively, and a sinusoidal curve is adjusted so as to fit them best.

sinusoidal curve with respect to the coordinate system of azimuth and elevation referred to the loci of the nose and tail of the rocket. Fig. 17 indicates the distribution of peak positions of X-rays for each spin during the period of a precession. The dashed lines in the upper and lower panels are the locus of the nose and that of the tail of the rocket, respectively. The hollow circles indicate the peak positions of X-ray sources seen during the preceding half a spin and full circles indicate those during the following half a spin.

The time interval from the moment when either of the two counters looks at a certain area of X-ray source during the preceding half a spin to the successive moment when the same counter scans again over the same location during its following half spin is only about 5 sec (since the double conical angle is 90°), so we can expect that the temporal change in source position during this time is quite small, and accordingly that the peak should appear at the same position independent of the scanning mode of either of the preceding half a spin or the following half. That is to say, the hollow and full circles in Fig. 17 should be on a common sinusoidal curve if the phase of the spin is correctly adjusted. Fig. 17 is a presentation of the common sinusoidal traces thus adjusted. A comparison between the curve seen by the F-counter (upper panel) and that by the B-counter (lower panel) tells us another important fact, since the two sinusoidal curves seen in both the F- and B-counters should be identical in space. As seen in the figure, the amplitude of the curve ranges from 9° to -26° in

elevation with respect to the nose locus (dashed line in the upper panel) whereas it ranges from 18° to -17° with respect to the tail locus (dashed line in the lower panel). This means that the loci of nose and tail are not exactly identical. Instead, they make an angle of 9°, both of them being 4.5° apart from the equator of the precession. The half a conical angle of the precession is thus accurately estimated to be 85.5°, while the zenith angle of the precession axis is estimated to be 17.5° from the half amplitude of the sinusoidal curve. The azimuthal angle of the precession axis was calculated from both the geomagnetic aspect and X-ray records independently to be 170° (geomagnetic 215°). Thus fairly accurate information for the flight attitude of the rocket along with the phase angle of each spin are known, and we are ready to compose the iso-photo maps of X-rays in space.

The composition of the iso-photo maps is achieved by a transformation of the coordinates from the precession coordinates in Fig. 17 to those of the real space. The transformation is simply realized by modifying the nose and tail loci from the straight lines in Fig. 17 to sinusoidal curves with the phase being the reverse of the X-ray source curve in the same figure, since the X-ray sources lie on a horizontal straight line for the observation period when the auroral arc had gone far enough away (later part of the flight). Fig. 18 represents an example of an iso-photo map thus composed. This is a map of 1/20-spin counts observed by the F-counter at each of its preceding half a spin during the third precession. Since the precession period is 20.47 sec, it takes 20.47 sec for the map to be completed by a full azimuthal scan of a counter with every half a spin, beginning at the right-hand side and ending at the left-hand.

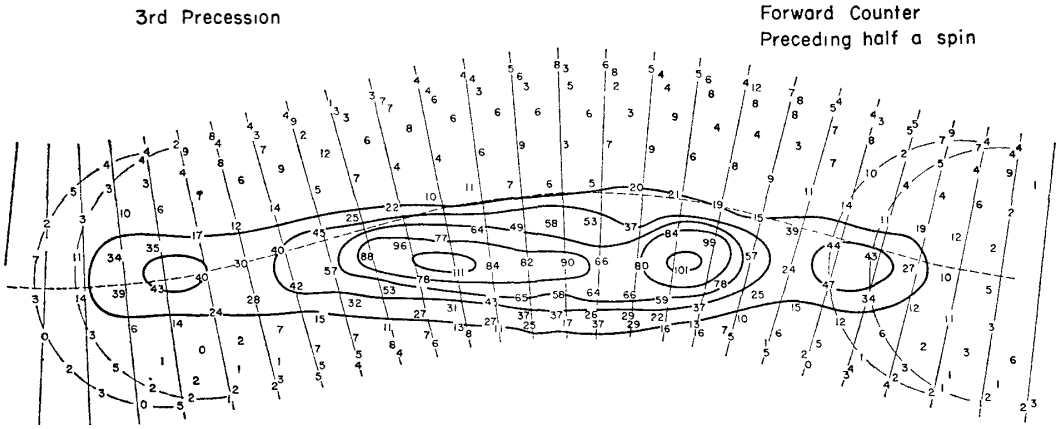

Fig. 18. An example of the iso-photo contour maps composed by using a number of 1/20-spin counts of auroral X-rays obtained from the forward counter alone, where data from the preceding half a spin group during the 3rd precession are plotted along a half circle each. The resulatnt contour lines are drawn by a 20 counts step. The dashed line is the nose locus of the rocket.

However, the preceding half a spin is followed by the following half a spin of the same counter with a phase delay of about $\pi/2$ ($\sim$ 5 sec), and this in turn is followed by the next preceding half a spin of another counter with a phase delay of also about $\pi/2$ ($\sim$ 5 sec), and so on. Thus, one fourth of a precession period is sufficient for making an iso-photo map of X-rays. Therefore, an iso-photo map can be composed by four quadrant scannings, for example, by the preceding half a spin of the F-counter from south to east, by the following half of the same counter from west to south, by the preceding half a spin of the B-counter from north to west, and by the following half of the B-counter from east to north. The iso-photo maps thus obtained for each one fourth precession are given in Fig. 19.

Each of the iso-photo maps in Fig. 19(a)-(k) consists of four parts; two come from a counter and the rest are the results from the other counter. In addition, there is a time gap of about 5 sec between any one part and the adjacent, because 5 sec is required for a counter to scan over one part from right to left. This, as well as the change in the counter from one part to the next, may result in considerable discontinuities of the contour lines, if rapid temporal and spatial variations of X-rays are included. This is the reason why the contour lines in Fig. 19 are left separated into four parts with small gaps in between.

Fig. 19 covers all the results of the X-ray distributions during the flight time from the nose cone removal to the telemeter off. Although we should have maps of 4 times the total precession number, 44 maps were composed by omitting the two precessions during which low signal to background ratios arose in low altitudes. The horizontal reference line of each map represents the horizon of the rocket, and accordingly the sequential maps clearly visualize the relative variation of the source altitude with respect to the rocket altitude. At the very beginning of the observation, the X-ray sources are distributed about 20° above the horizon of the rocket. This was expected from the relative position of the rocket to the aurora at that time, since the auroral arcs were located nearer to the zenith when the rocket attained 70 km altitude in its ascent. The average altitude of the sources was then gradually lowered with respect to the rocket horizon as the rocket came up, and it almost overlapped the horizon when the rocket reached the 110 km level. After that, the rocket looked at the X-ray sources below its horizon, until it came down again to the same level about 2 seconds later. This fact suggests that most of the X-ray sources were concentrated near 110 km in height. Furthermore, the auroral arcs were located very far from the rocket during its descent, so that the increasing rate in elevation of the sources during its descent was much smaller than the decreasing rate during its ascent. Such a tendency is consistent with the change in distance of the auroral arc estimated from all-sky photographs.

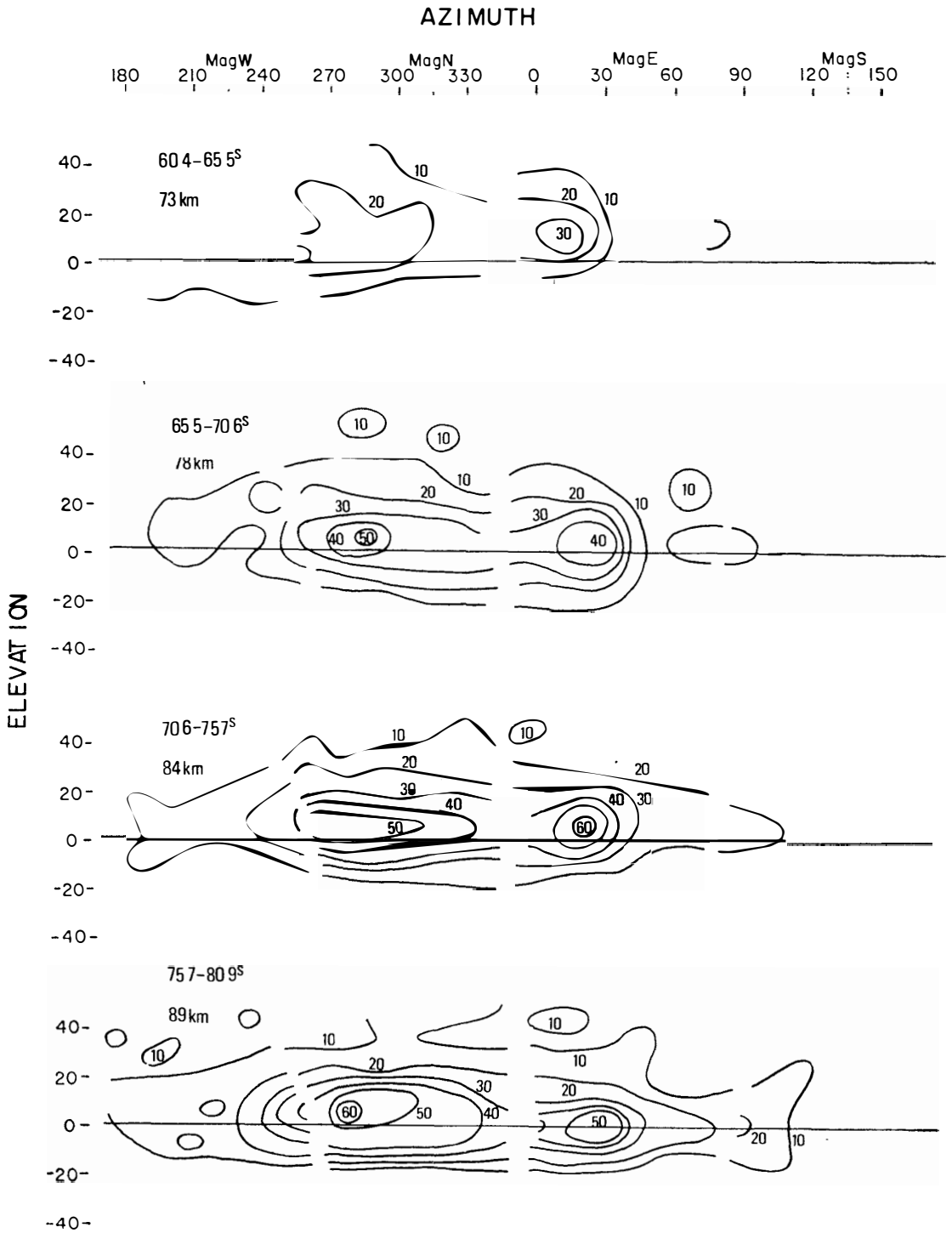

Fig. 19(a)-(k). A sequence of iso-photo maps of auroral X-ray intensities composed every 5 sec by using all the data from both the forward and backward counters. Numerical figures attached on contour lines indicate the 1/20-spin counts of the X-rays. The time and altitude after launch are also given in each map.

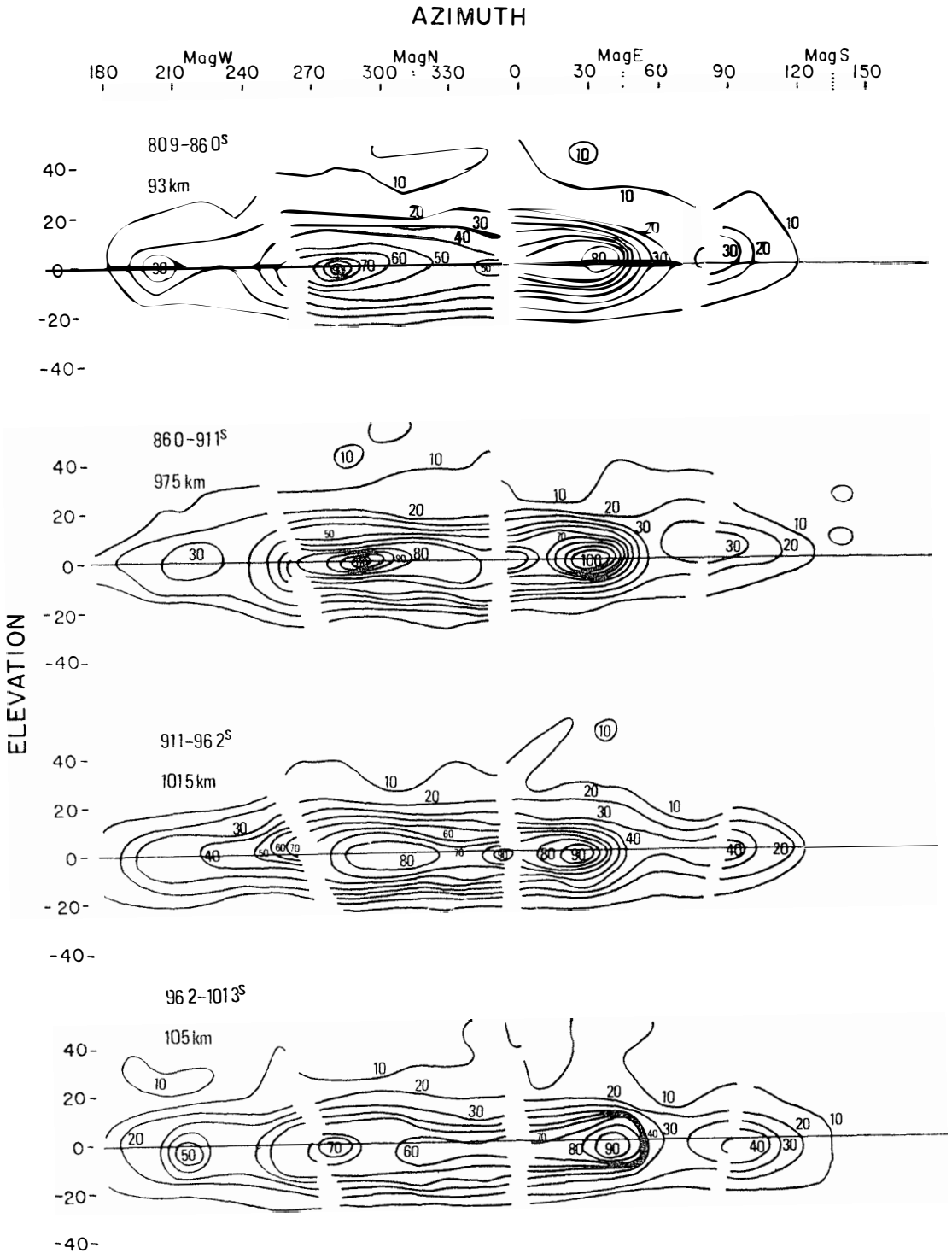
AZIMUTH
MagW
MagN
MagE
MagS
180 210 240 270 300 330 0 30 60 90 120 150
809-860S
93km
860-911S
975km
911-962S
1015km
962-1013S
105km
ELEVATION
40
20
0
-20
-40

Fig. 19(b)

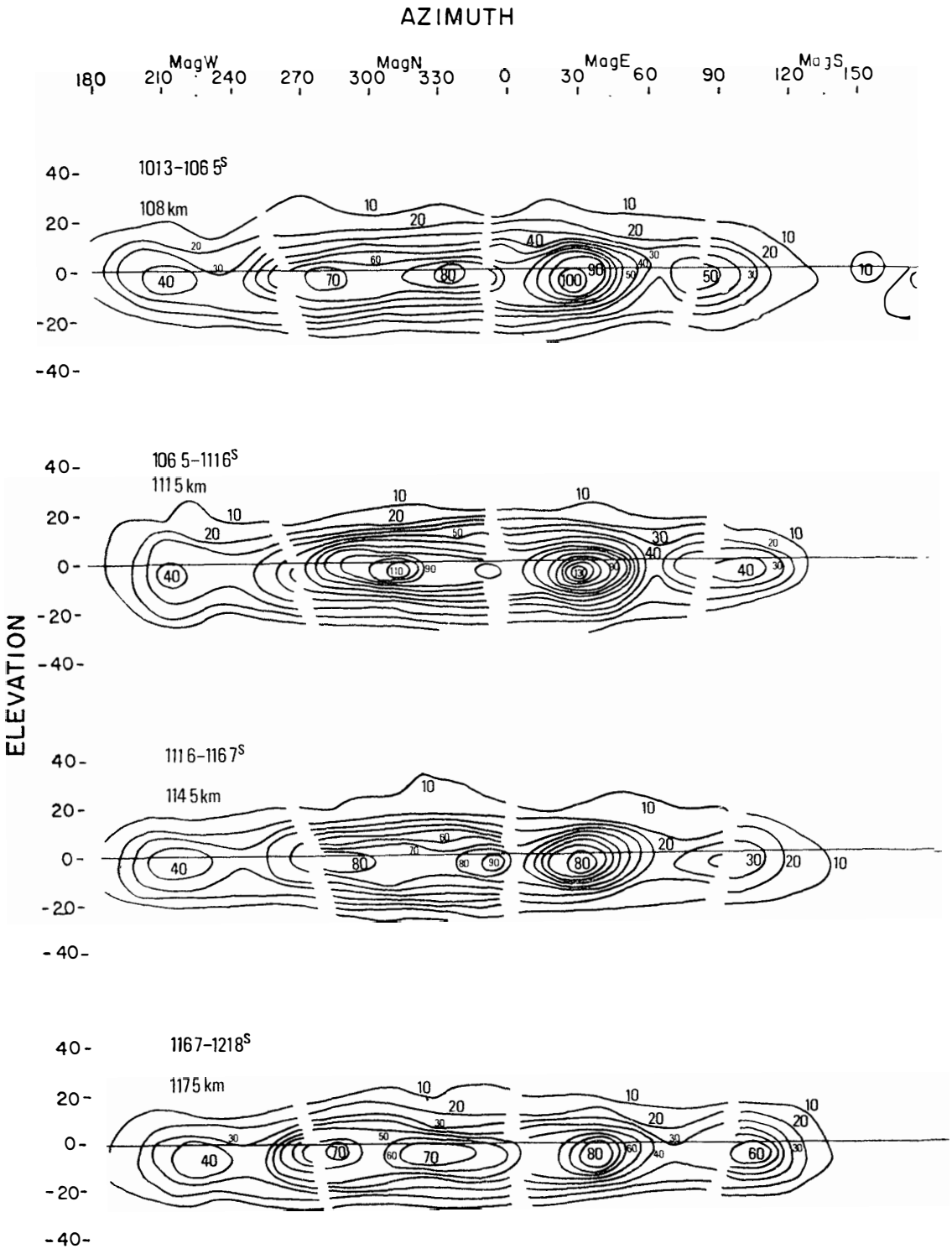
AZIMUTH
MagW
MagN
MagE
MagS
180 210 240 270 300 330 0 30 60 90 120 150
ELEVATION
40
20
0
-20
-40
1013-1065S
108 km
1065-1116S
1115 km
1116-1167S
1145 km
1167-1218S
1175 km

Fig. 19(c)

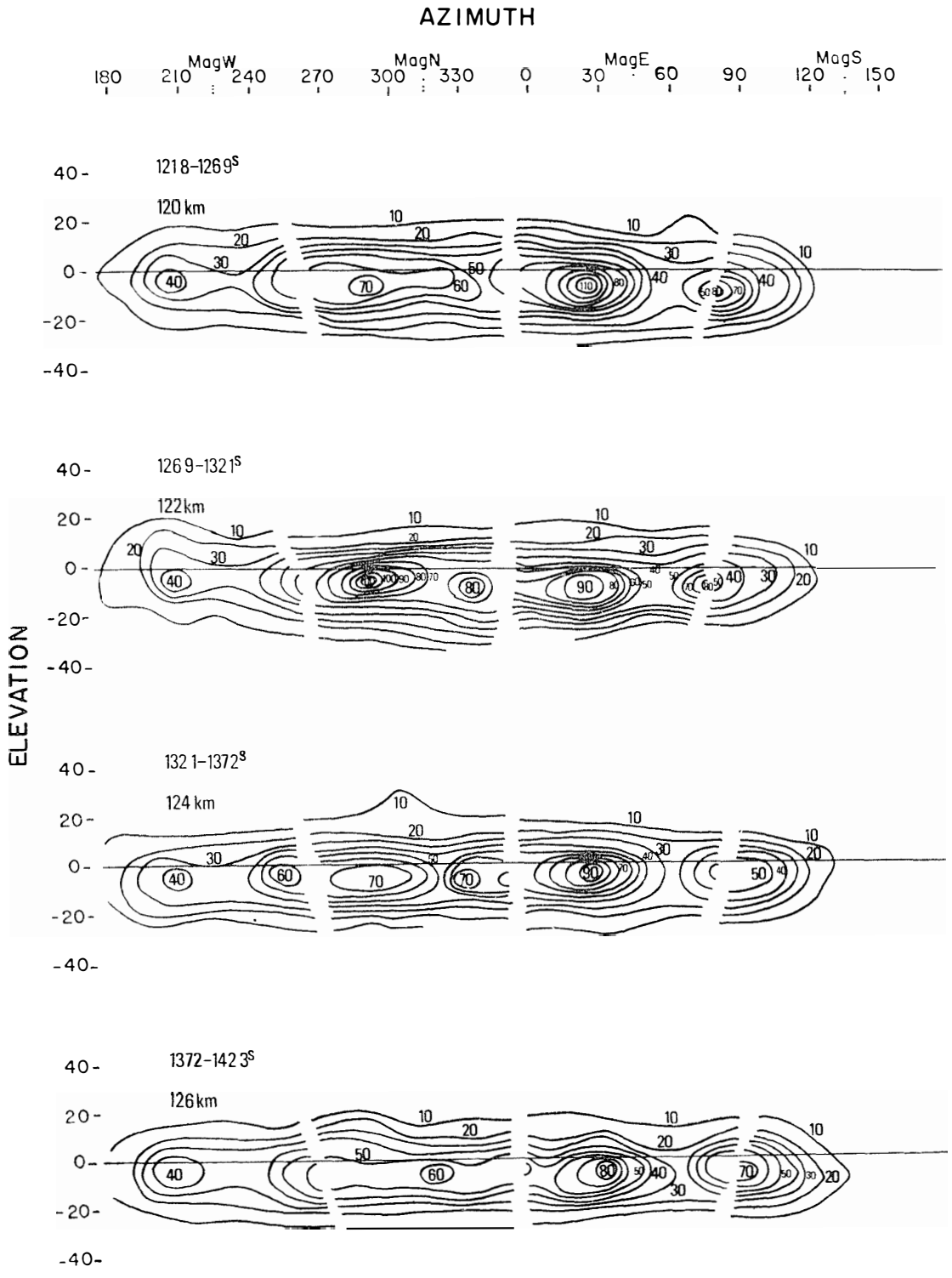
AZIMUTH
MagW
MagN
MagE
MagS
180
210
240
270
300
330
0
30
60
90
120
150
ELEVATION
40
20
0
-20
-40
1218-1269S
120 km
1269-1321S
122km
1321-1372S
124 km
1372-1423S
126km

Fig. 19(d)

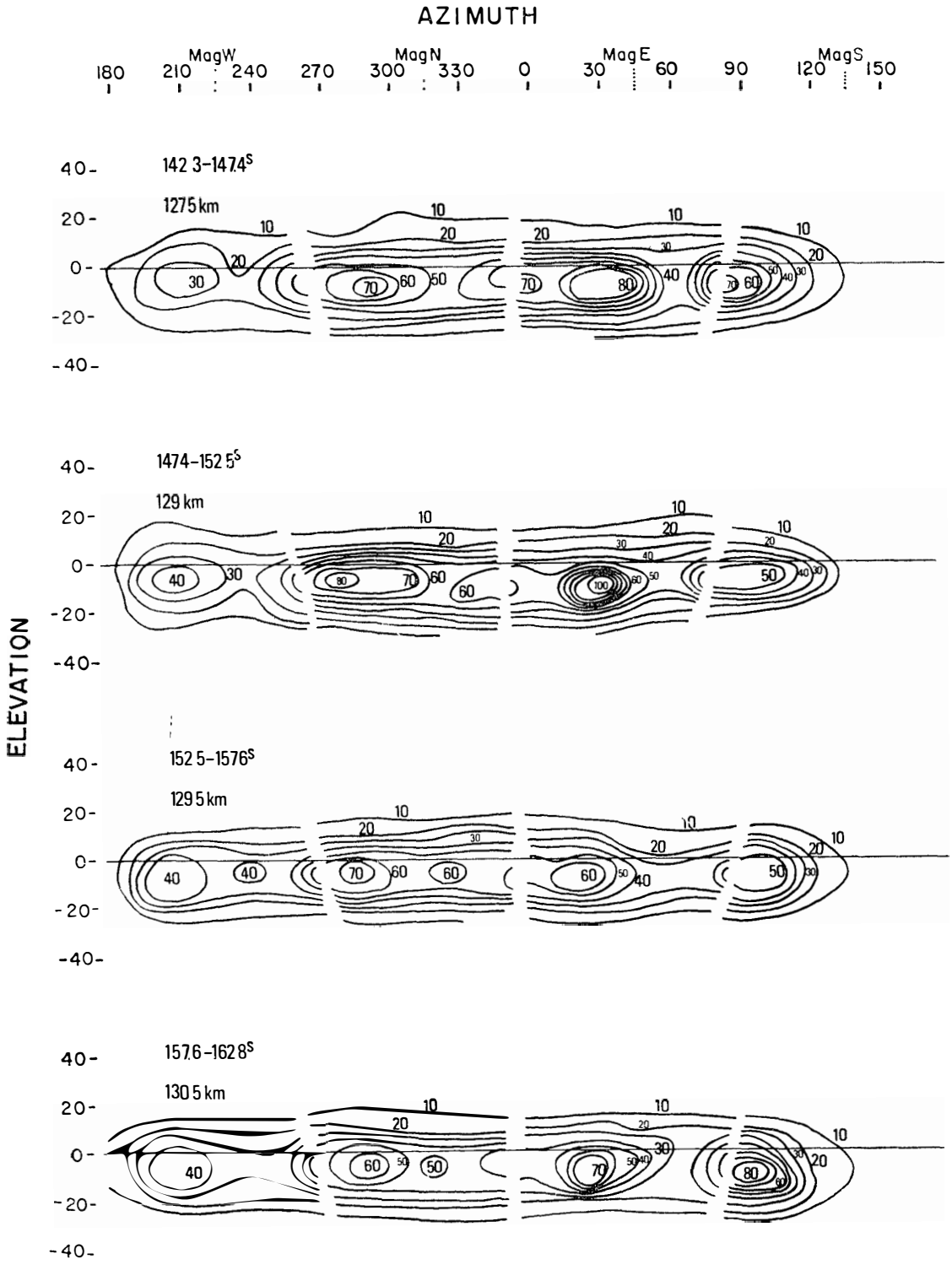
AZIMUTH
MagW
MagN
MagE
MagS
180
210
240
270
300
330
0
30
60
90
120
150
ELEVATION
40
20
0
-20
-40
142 3-147.4°S
127.5 km
147.4-152.5°S
129 km
152.5-157.6°S
129.5 km
157.6-162.8°S
130.5 km

Fig. 19(e)

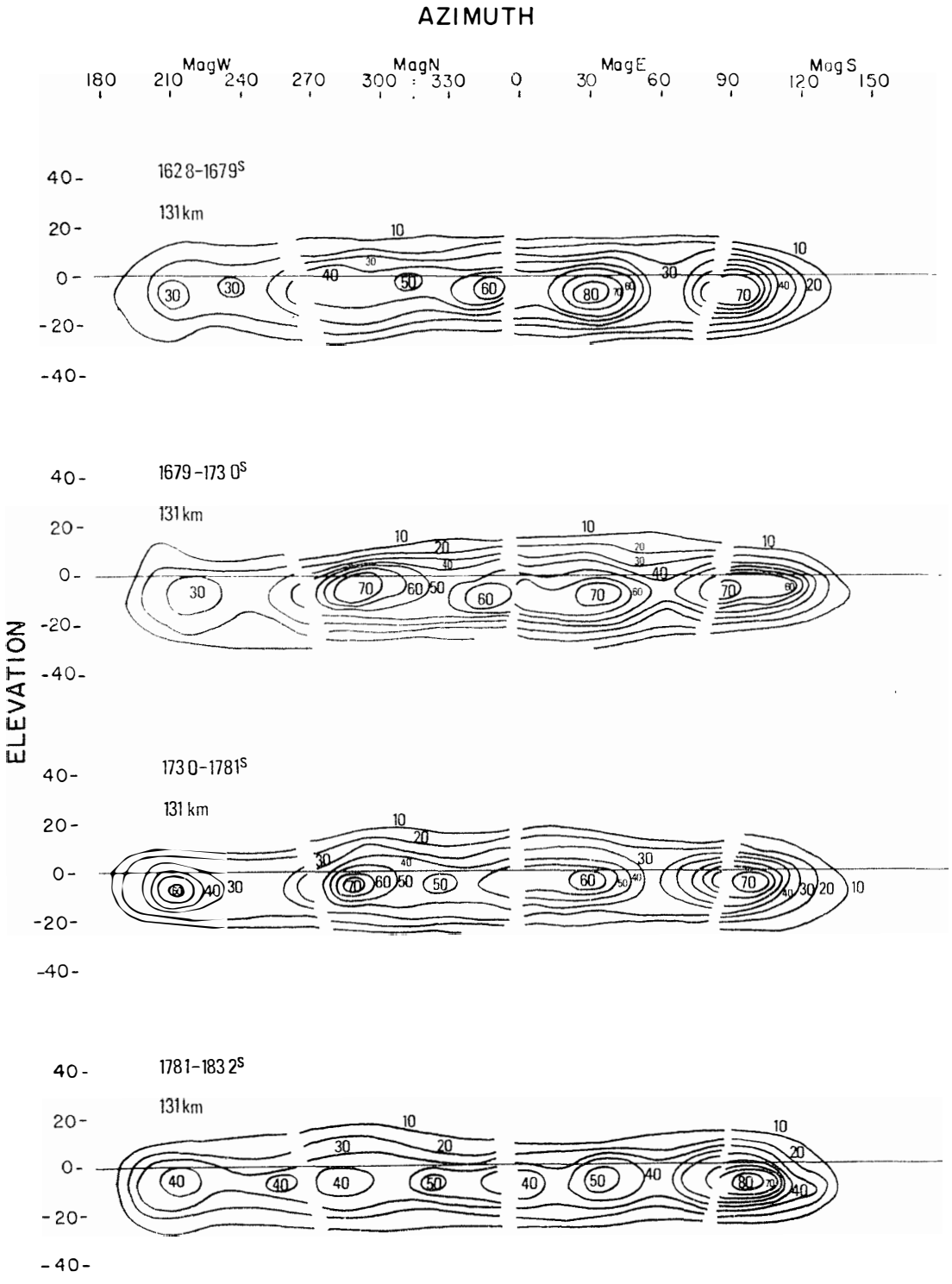
AZIMUTH
MagW
MagN
MagE
MagS
180 210 240 270 300 330 0 30 60 90 120 150
ELEVATION
40
20
0
-20
-40
1628-1679S
131km
1679-1730S
131km
1730-1781S
131km
1781-1832S
131km

Fig. 19(f)

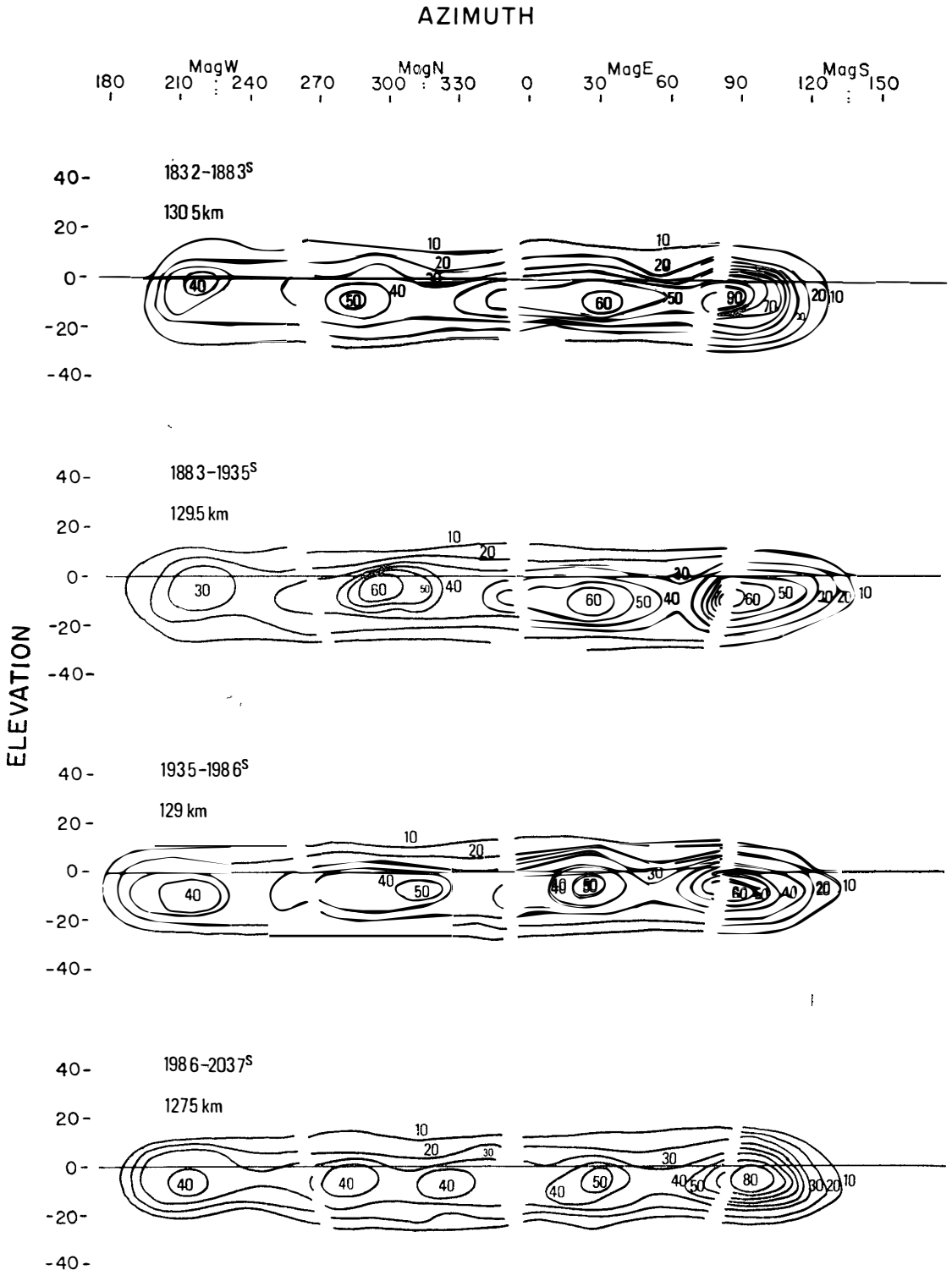
AZIMUTH
MagW
MagN
MagE
MagS
180 210 240 270 300 330 0 30 60 90 120 150
ELEVATION
40-
20-
0-
-20-
-40-
1832-1883S
1305km
1883-1935S
129.5 km
1935-1986S
129 km
1986-2037S
1275 km

Fig. 19(g)

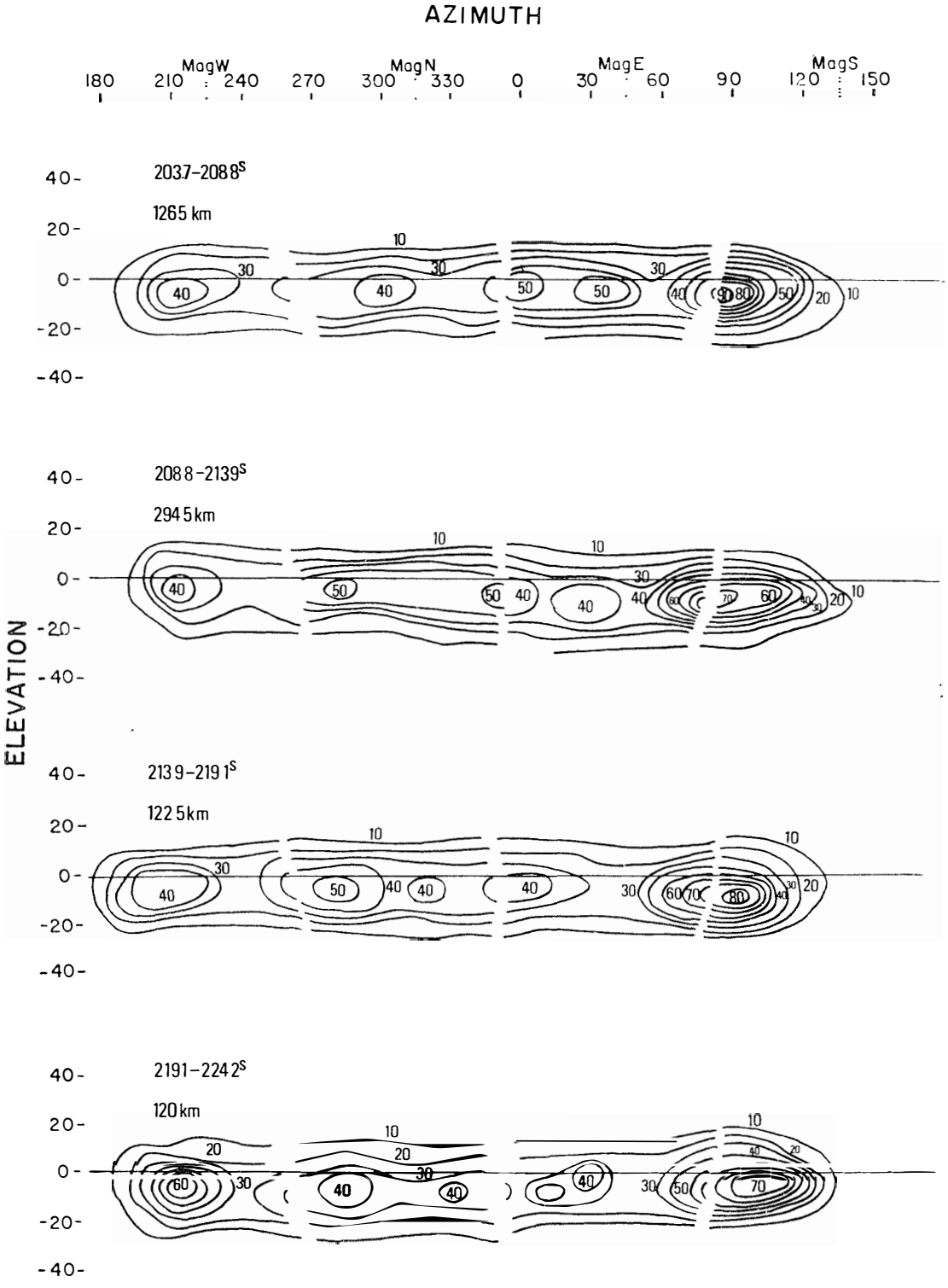
AZIMUTH
MagW
MagN
MagE
MagS
180 210 240 270 300 330 0 30 60 90 120 150
ELEVATION
40
20
0
-20
-40
2037-2088S
1265 km
2088-2139S
2945 km
2139-2191S
1225 km
2191-2242S
120 km

Fig. 19(h)

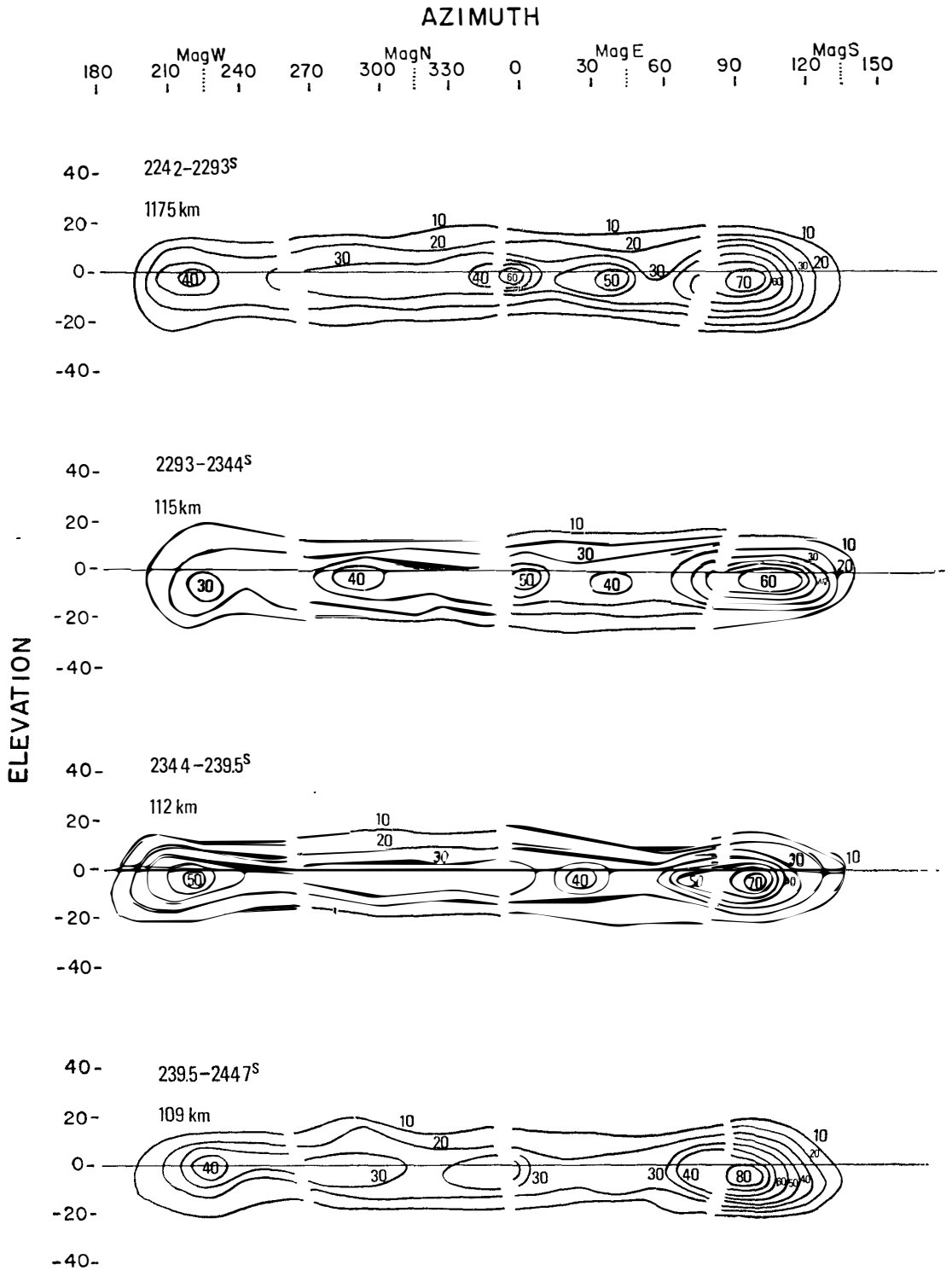
AZIMUTH
MagW
MagN
MagE
MagS
180
210
240
270
300
330
0
30
60
90
120
150
ELEVATION
40-
20-
0-
-20-
-40-
224.2-229.3S
1175 km
229.3-234.4S
115 km
234.4-239.5S
112 km
239.5-244.7S
109 km

Fig. 19(i)

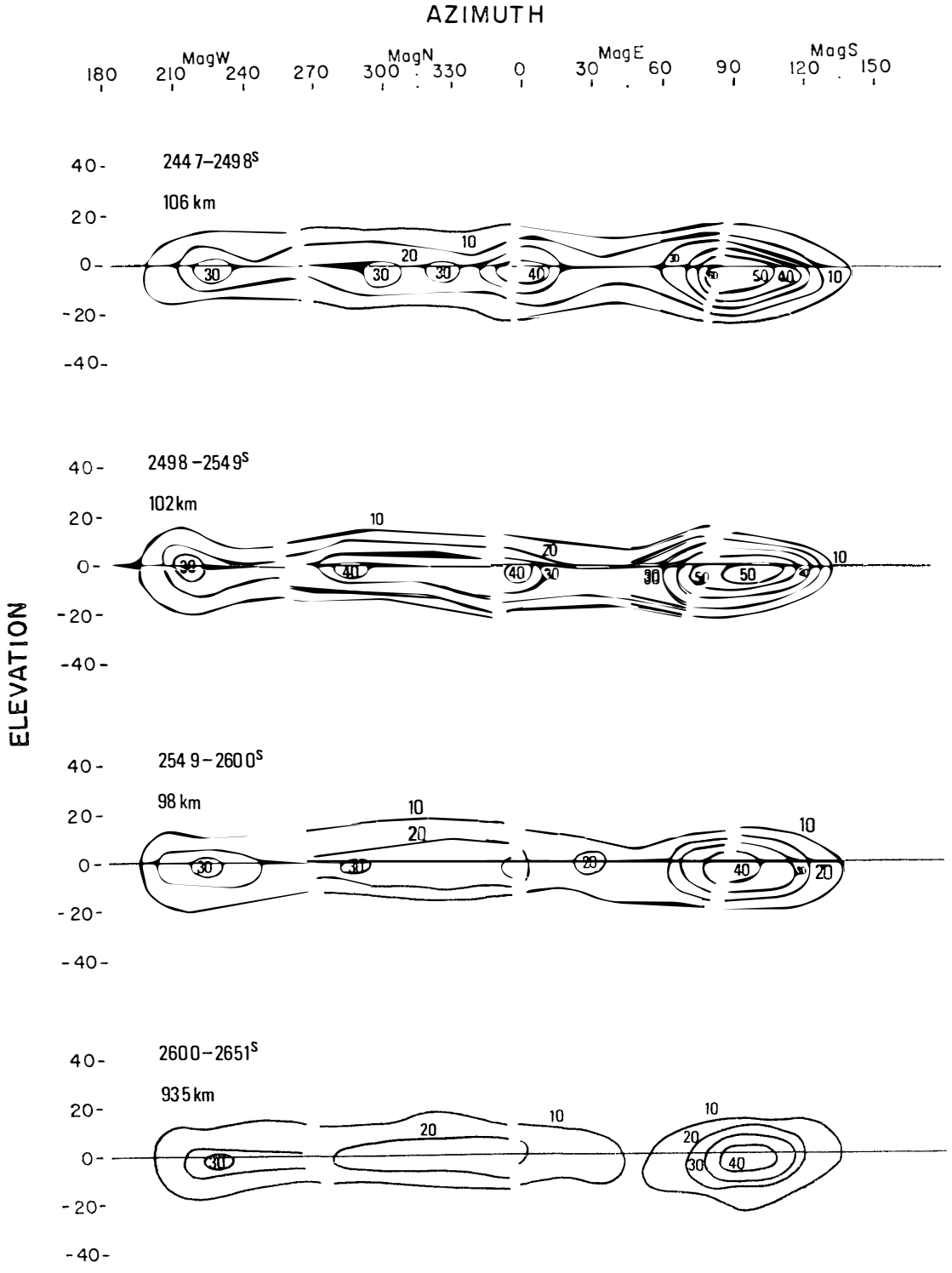
AZIMUTH
180
MagW
210
240
270
MagN
300
330
0
MagE
30
60
90
MagS
120
150
ELEVATION
40
20
0
-20
-40
2447–2498S
106 km
2498–2549S
102km
2549–2600S
98 km
2600–2651S
935 km
10
20
30
40
50

Fig. 19(j)

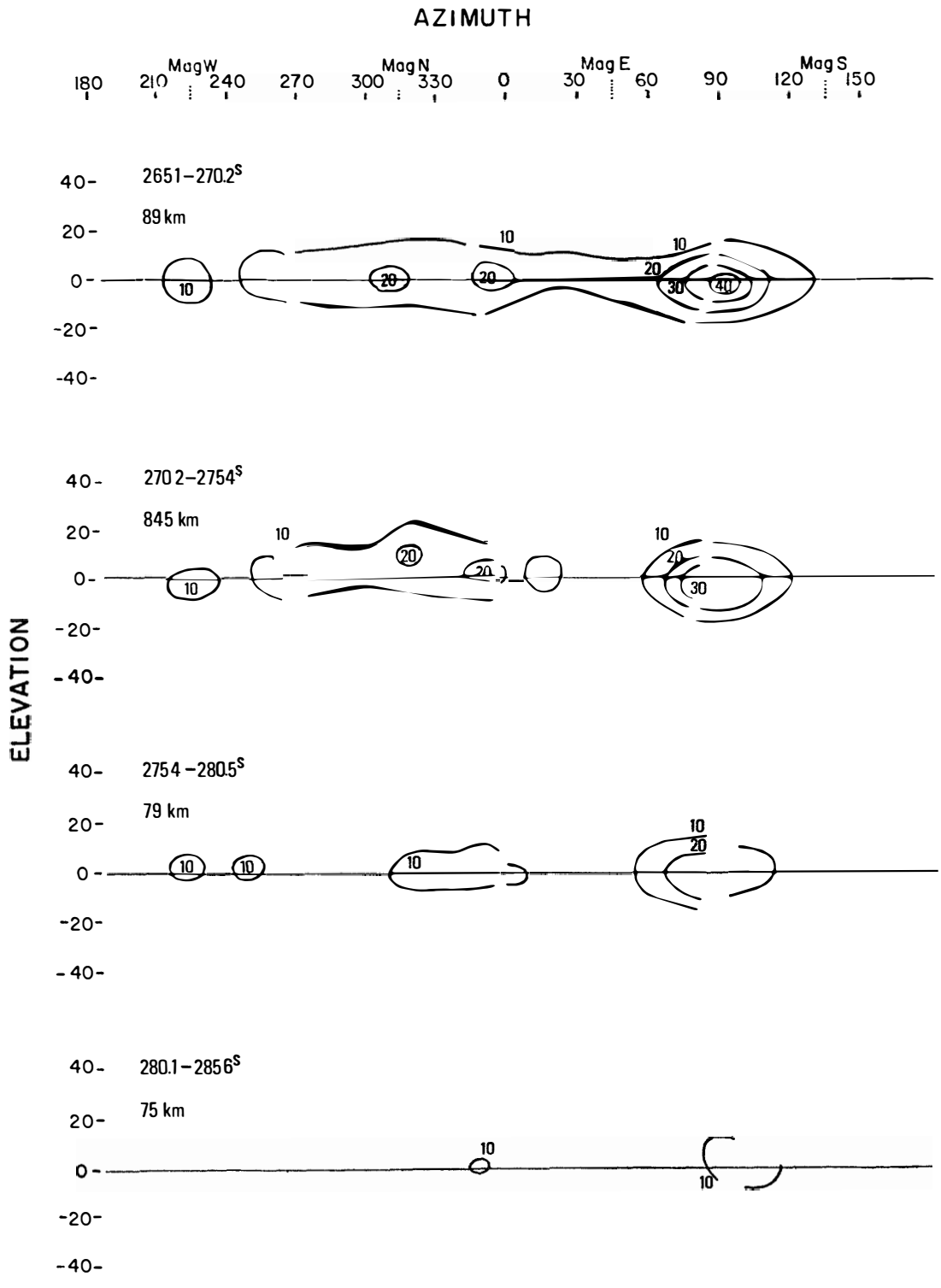
AZIMUTH
180
210
MagW
240
270
300
MagN
330
0
30
Mag E
60
90
120
Mag S
150
ELEVATION
40-
20-
0-
-20-
-40-
265.1–270.2S
89 km
270.2–275.4S
845 km
275.4–280.5S
79 km
280.1–285.6S
75 km
10
20
30
40

Fig. 19(k)

Another important fact seen from the sequential maps is the existence of local enhancements of X-ray intensity along the visual auroral arcs. Corresponding to the fact that bright auroral arcs situated in the close north-east vicinity of the rocket during its ascent, the X-ray distribution is spread upward with its center at approximately 20° above the rocket horizon in the north-east. The strong X-ray sources from north to east correspond to the auroral activities along arcs seen in all-sky photographs in Fig. 8. The fold structures also are likely to be identical with the strong X-ray source regions.

Let us examine further the azimuthal distribution of the X-ray sources. The patch-like patterns of Fig. 19 imply the existence of several points of X-ray sources whose intensities are different from source to source. In order to easily see time characteristics of the point sources throughout the entire flight time, the space-time chart of Fig. 20 was composed using all of the maps. It is likely that there exist at least five sources along the azimuthal directions as indicated by S1, S2, S3, S4 and S5. Also, it should be noted that the X-ray intensities from the individual sources are not always stable with time but are rather changeable. In Fig. 21, such dissimilar time profiles can easily be seen from each of the sources.

It is evident from Fig. 20 that the two sources in the east-south-east (S1) and in the south-west (S5) generally tended to become relatively intense as the rocket came up. Although the north-eastern part (S2) was the most intense

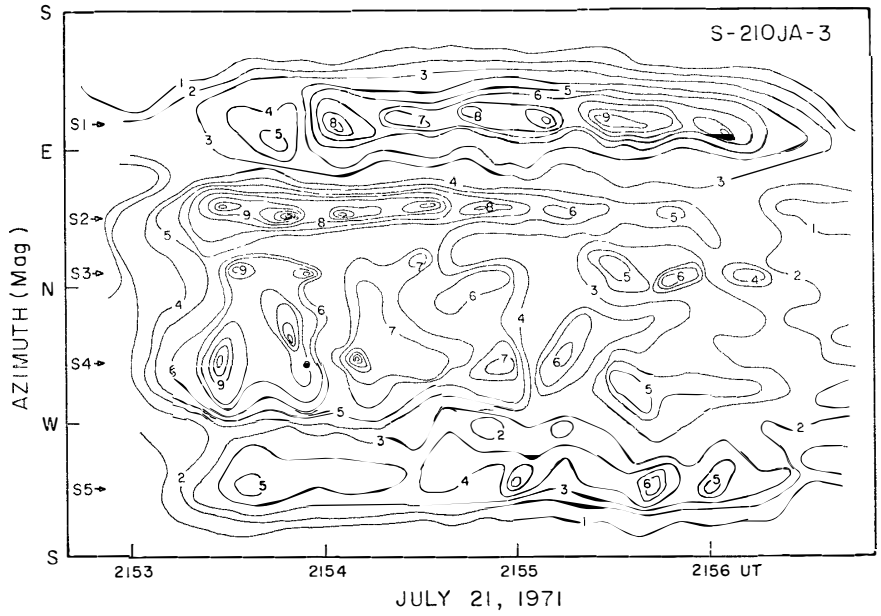

Fig. 20. A space-time chart of auroral X-ray intensities viewed from the rocket altitude. Localized intensity enhancements are significant in the five azimuthal directions indicated by arrows.

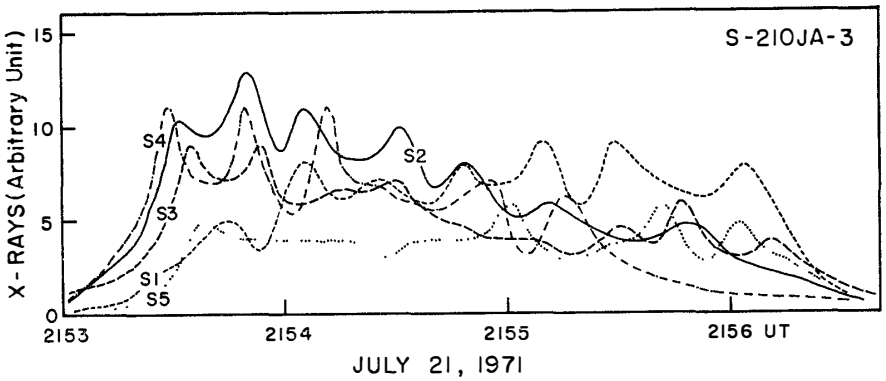

Fig. 21. Intensity-time profiles of auroral X-rays taken from five sources located in positions S1, S2, S3, S4 and S5 of Fig. 20.

during the first half of the flight, it decreased fairly rapidly leaving the eastern and the south-western sources dominant in the last phase of the flight. This fact reveals that the X-rays were intense in roughly the east-west direction, namely, along the auroral oval because of a spatial integration along the line of sight, after the decay of the local activity (S2, S3 and S4) in the north. The superimposed periodic intensity variations, being roughly 20% in amplitude, are not real. Most of them came from the unequal sensitivity of the F- and B-counters which was estimated from Fig. 16 to have an average 20% difference and which apparently modulated the observed intensities with a period of ~ 20 sec synchronous to the precession.

7. Similarities and Dissimilarities between Auroral X-Ray and Ultraviolet Emissions

Another rocket-borne instrument was operated to measure ultraviolet (UV) emissions associated with the auroral activity. A UV detector, consisting of an ionization chamber sensitive to radiations from 1100 Å to 1360 Å and giving a circular viewfield of 10°, was mounted so as to place its optical axis parallel to the rocket spin axis (TOHMATSU *et al.*, 1974). Because of the large precession motion of the rocket as described earlier, the UV detector scanned along the nose locus of the rocket. Accordingly, the line of sight of the detector twice crossed the auroral arc lying near the rocket horizon every precession. It resulted in two distinct enhancements of UV emissions during a precession.

In order to compare UV emissions with X-rays, it is necessary to trace the X-ray intensities from the F-counter along the nose locus, or along the tail locus for the B-counter. This can easily be done from a series of diagrams similar to Fig. 18. In this way, we can obtain four independent time profiles every precession, from the preceding and following half a spin each for the F-counter

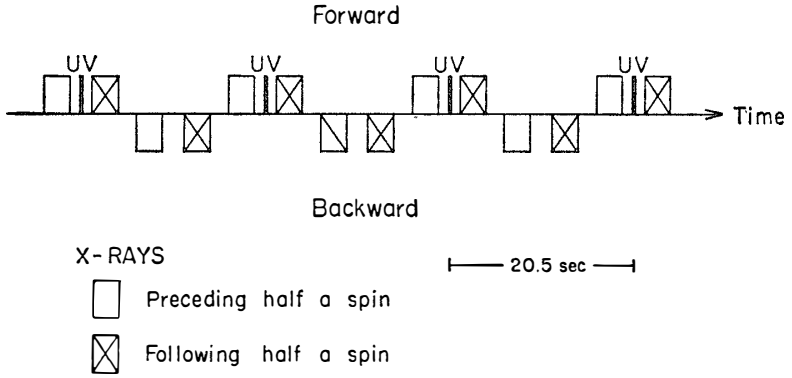

Fig. 22. The time relation in viewing directions among the three detectors, one of which is for ultraviolet emissions and the other two for auroral X-rays. The aperture angle of each detector is expressed roughly by the width of the rectangle.

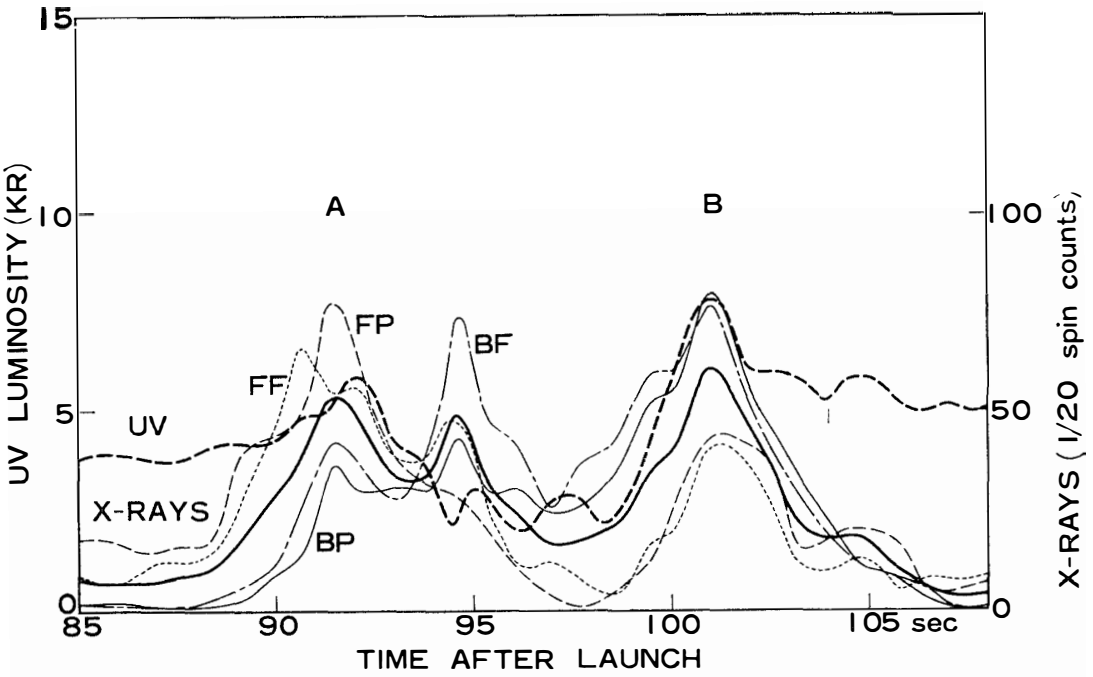

Fig. 23(a)-(h). Intensity variations of ultraviolet and auroral X-ray emissions along the nose or tail locus of the rocket. The locus crossed the auroral arc twice, at positions A and B. Since a certain part of space is scanned twice by each of the two X-ray counters during a precession, the corresponding four curves are drawn, together with their average (thick solid line): FP is labeled for the preceding half a spin of the F-counter, BF for the following half a spin of the B-counter, and so on.

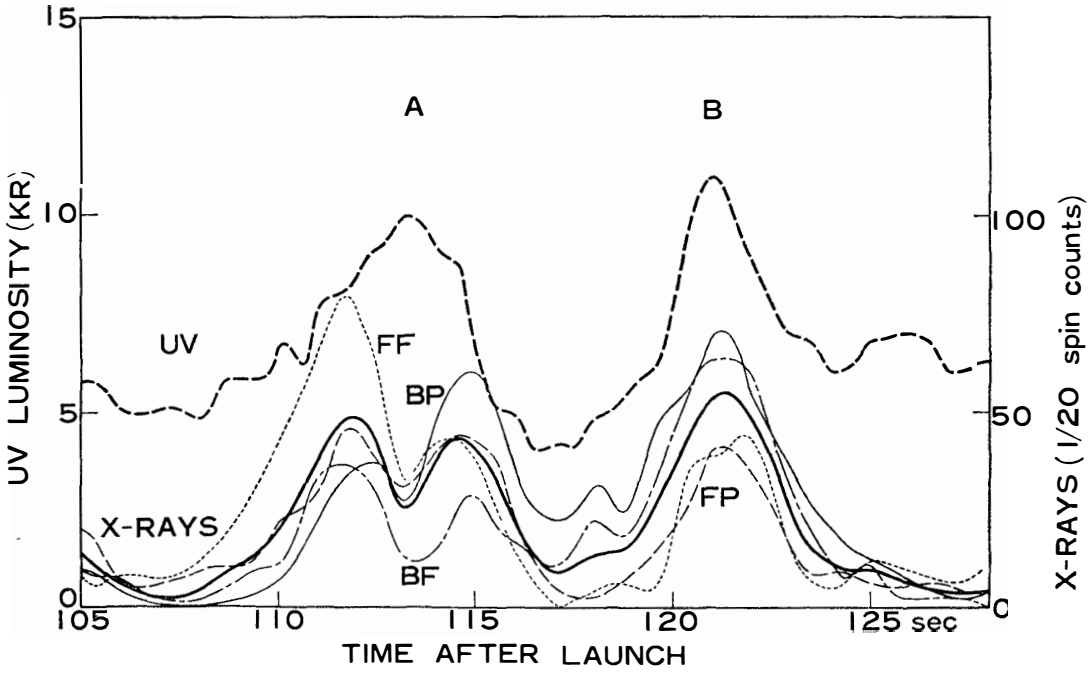

Fig. 23(b)

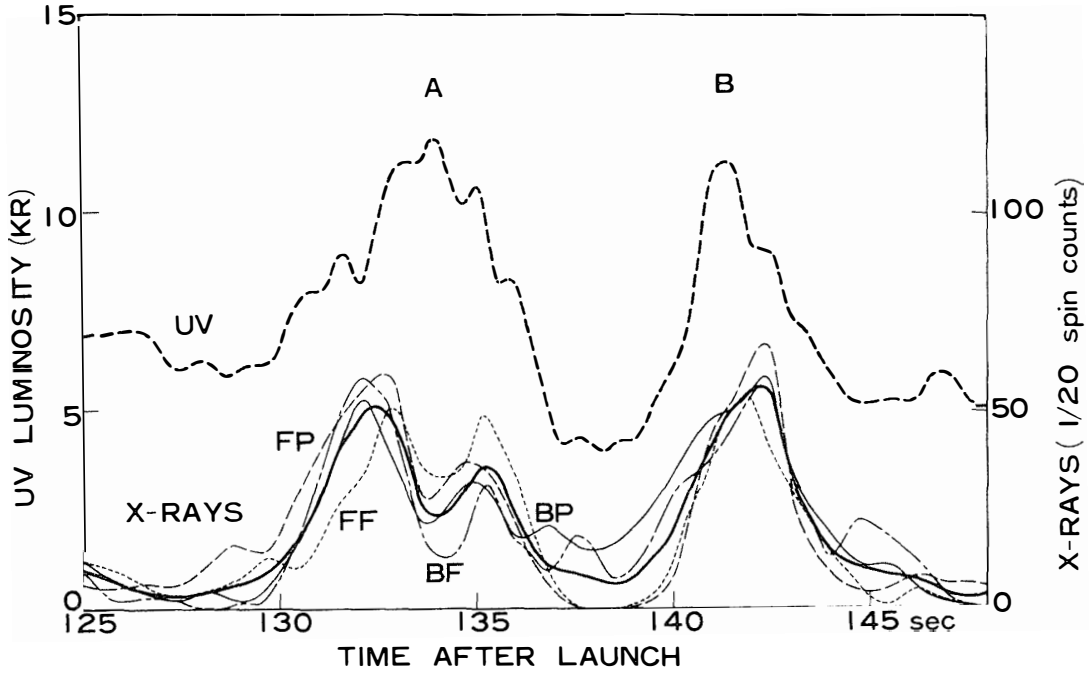

Fig. 23(c)

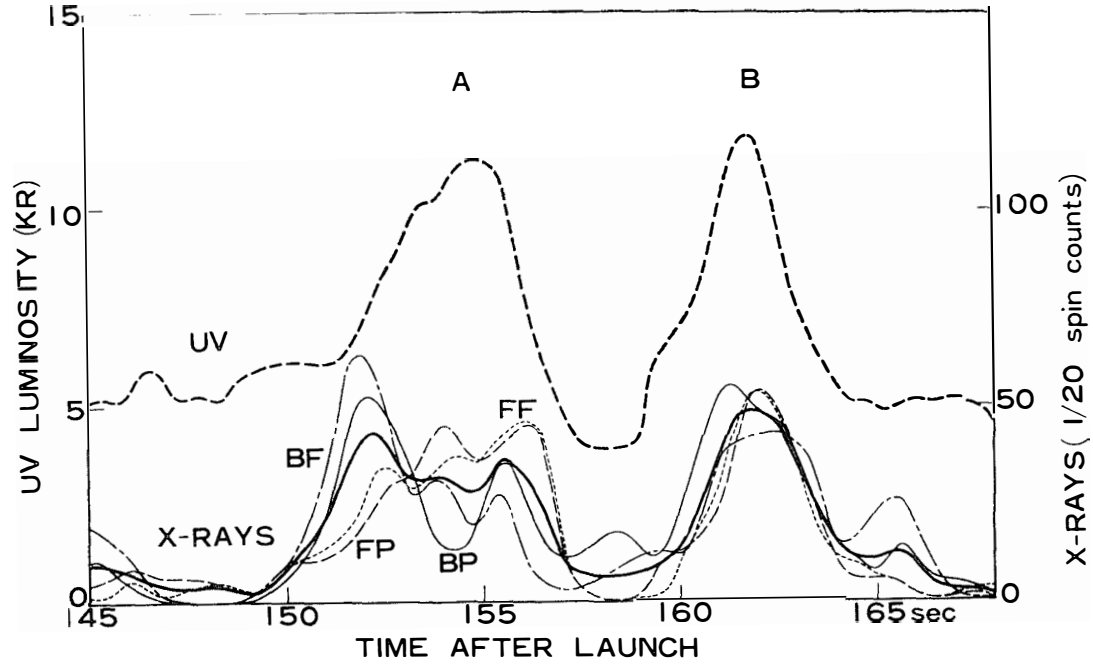

Fig. 23(d)

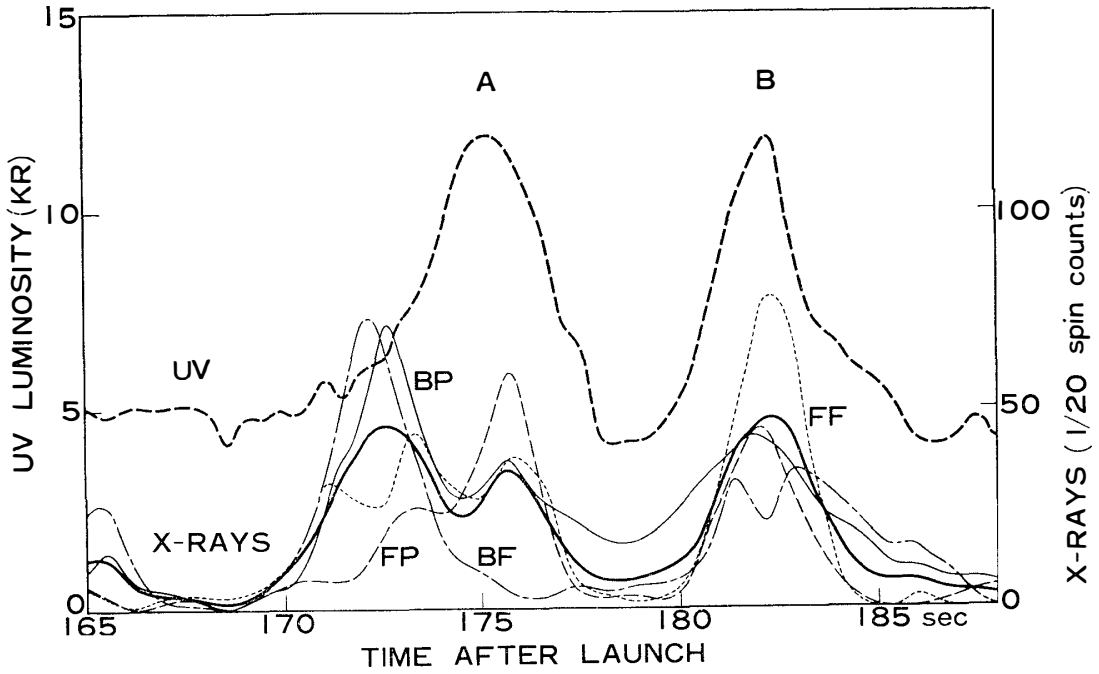

Fig. 23(e)

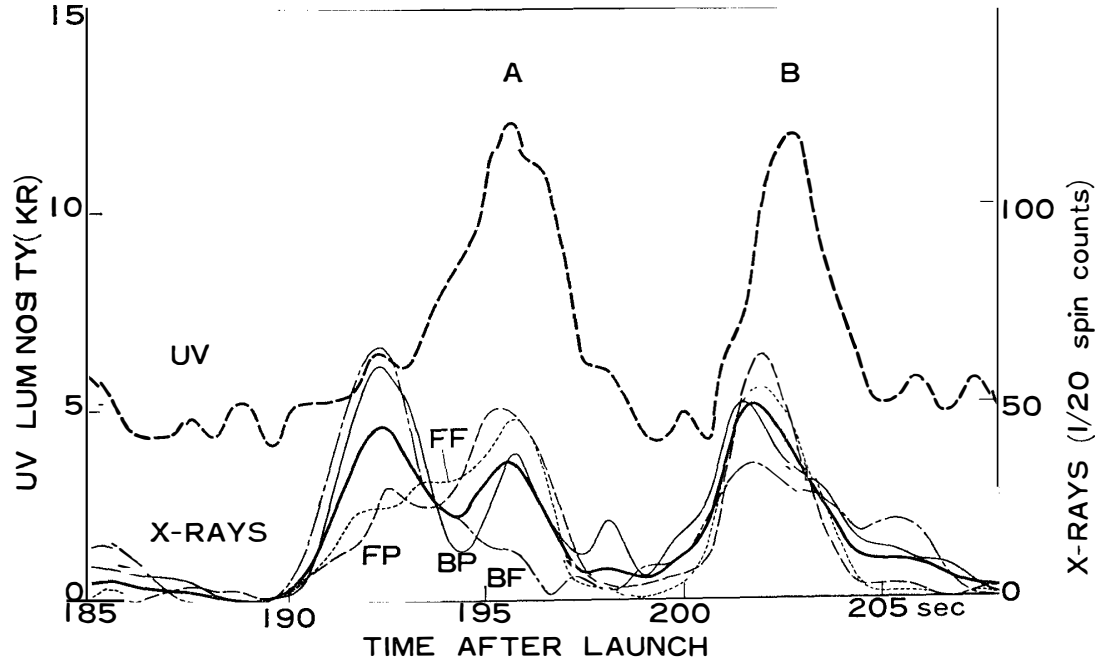

Fig. 23(f)

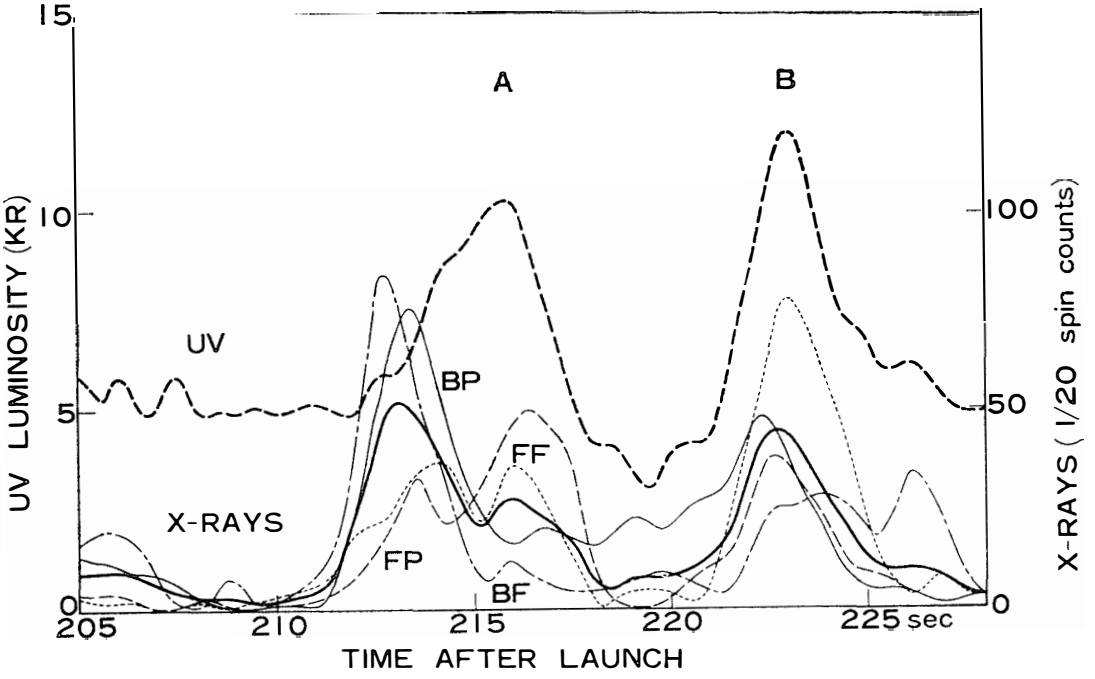

Fig. 23(g)

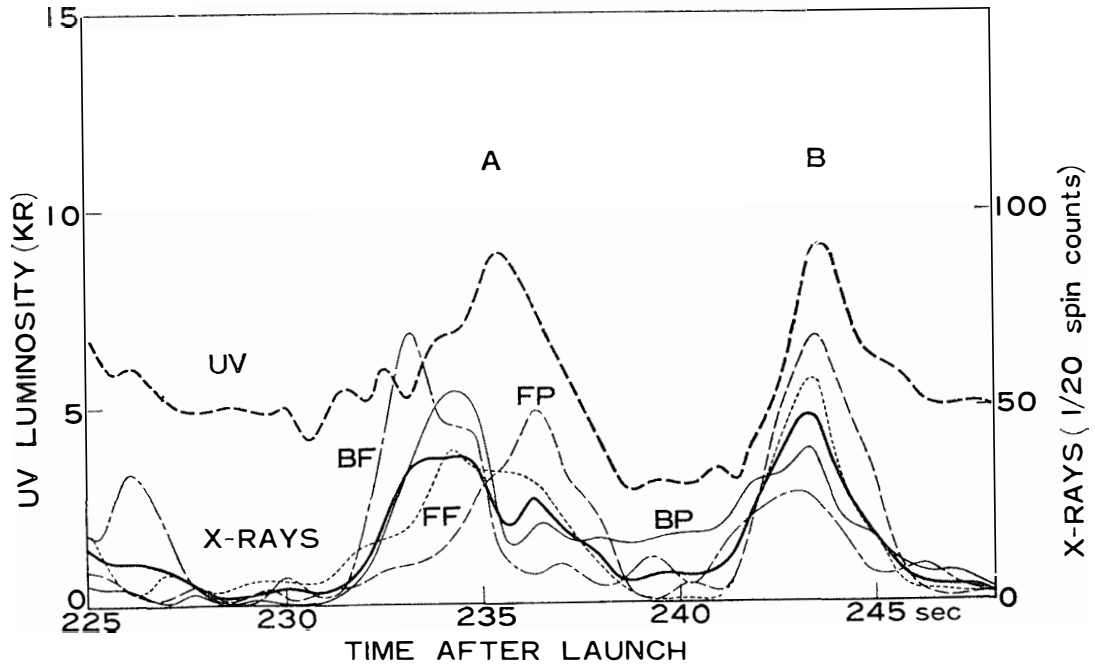

Fig. 23(h)

and also from each similar spin for the B-counter. It should be noted that the preceding half a spin is ~ 2.5 sec in advance phase of the UV scanning which is again ~ 2.5 sec in advance of the following half a spin. In addition, there is a time gap of ~ 10 sec between the F- and B-counters. This situation in time sequence is illustrated schematically in Fig. 22.

All of the results obtained are shown in Fig. 23(a)-(h), together with the corresponding UV profiles. A general parallelism is well established between the time profiles of the UV and X-ray emissions, that is, spatial distributions viewed along the rocket spin axis during a round motion in the azimuth. However, there still exist some discrepancies due to temporal variations, which are, for example, significant in Fig. 23 (d). It is of interest that the time variations of X-ray intensities become occasionally larger. This suggests the existence of several local small sources of X-rays, whereas the diffuse background contributes much to UV emissions.

To examine further the above parallelism, the four curves of X-rays were simply averaged when ignoring the time difference of Fig. 22. The results are indicated by thick lines for every precession in Fig. 23 also. The good parallelism between both emissions is seen again for each peak position B but is not so clear for the other peak position A. Double humps of X-rays which appeared within peak A are obscure in the case of UV emissions. In addition, it is evident that the intensity ratio of X-rays to UV emissions changes very much in the A profile, being higher at the left-hand side and much reduced in the right-hand, whereas it shows the maximum near the center in the B profile. These behaviors are understood when the common, energy-dependent, auroral precipitation as well as the viewing angle of the two detectors are taken into consideration as in the following.

The two peaks of A and B represent the intensities at the regions where the nose locus intersects the auroral arc which is seen near the rocket horizon. On the basis of the rocket attitudes we readily realize that peak A comes from the western view while peak B comes from about 10 degrees east of the south in geomagnetic coordinates. The former is, therefore, along the auroral oval and the latter is almost perpendicular to the oval. Thus, the difference in the viewing direction may be expected to result in the different relations between profiles of X-ray and UV emissions at locations A and B, because profile A indicates a somewhat latitudinal survey of both emissions whereas B rather represents the spatial structure of the aurora.

The energies of the parent electrons corresponding to X-rays and UV emissions are of course not identical. The X-rays here represent the electrons with energy greater than 4 KeV and the UV here on the other hand represents electrons with lower energy, say less than 2 KeV if the excitation source is

electrons, as the altitude profile in Fig. 25 suggests. The auroral precipitation is commonly related to its energy. The lower energy electrons spread over a wider latitudinal range than the higher ones and are more abundant in higher latitudes. These characteristics together with the difference in viewing angle explain the double humps of X-rays with a single peak of UV emissions and the relatively high intensity of X-rays at the left-hand side of the A profile. Namely, the double humps of X-rays correspond to two lines of sight which include double arcs of aurora along with a single broad peak of UV emissions, and the high intensity relative to UV emissions in the left half of the A profile is ascribed to the relatively higher energy of precipitations in lower latitudes. On the other hand, the general correlation of the peak positions and the relatively higher ratio of X-rays at the center in the B profile are understood such that the precipitation is hard at the center, being consistent with common structure of the discrete auroral precipitation.

The dissimilarity between A and B is also found in the time profiles of their peak intensities. Picking up both the peak values, the long-term variations of UV and X-ray intensities identified at locations A and B are shown in Fig. 24. Peak intensities of X-rays in position B are somewhat higher than those in position A during the entire flight, but no significant difference between peaks A and B is found in UV emissions. Also, the feature of a gradual decay of X-rays is not found in UV emissions. These facts imply that the radiation

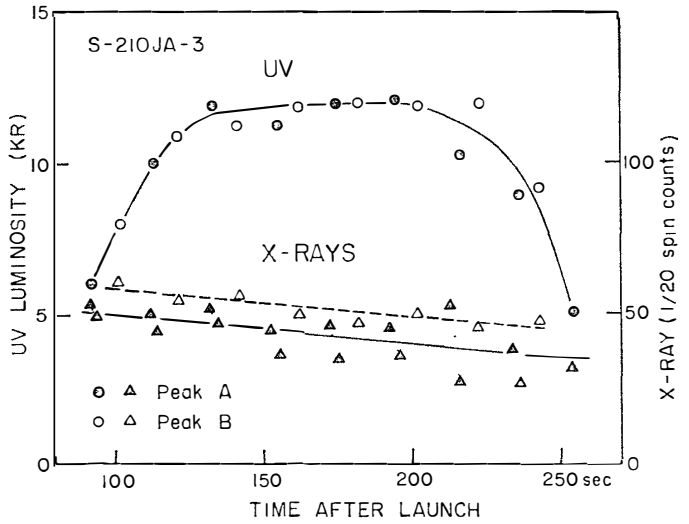

Fig. 24. Time profiles of peak intensities of ultraviolet and X-ray emissions in locations A and B of Fig. 23 during the entire flight. The pair of triangles correspond to the double humps in the X-ray profile A.

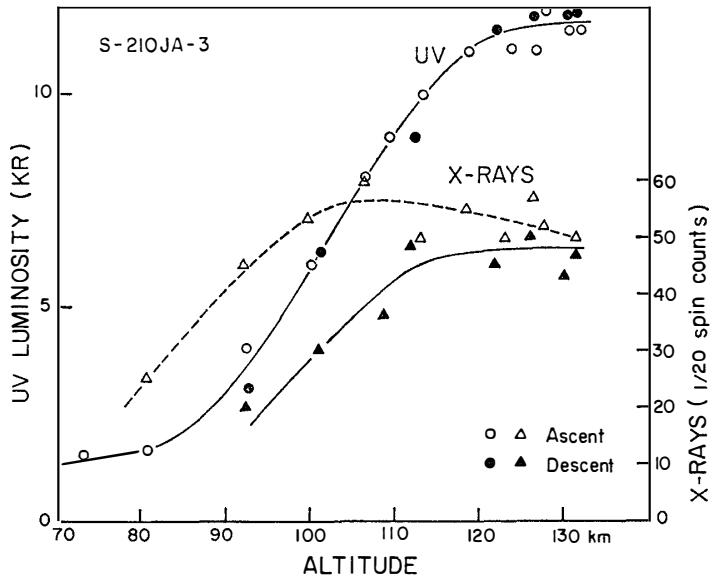

Fig. 25. Altitude dependences of ultraviolet and auroral X-ray emissions observed in the ascent and descent of the rocket.

configuration of X-rays is different between the vicinities of the A and B peaks although that of the UV emissions does not change as mentioned above, and that the decay rate here is higher for the precipitation with higher energy.

Further evident testifying to the inherent difference between UV and X-ray emissions is given by the altitude dependence indicated in Fig. 25. The UV intensities first saturated at over 130 km, while the X-rays began to saturate near 110 km. Moreover, the apparent ascent-descent difference, which was caused by the horizontal displacement of the auroral arcs in the case of X-rays, was negligible in the UV emissions. The former may be related to possible differences in the height of the production layer due to the difference in parents' energy and the propagation mechanism between both of the emissions. The latter is consistent also to the wide spread source of UV emissions with discrete sources of X-rays and to the more rapid decay of X-ray sources relative to UV emission sources as mentioned above.

8. Comparisons with Other Associated Auroral Phenomena

8.1. Luminosities

As is seen from Fig. 8, the auroral activity dropped gradually from time to time. Fig. 26 gives a quantitative representation of the general decay of X-ray intensity, for a pair of 1/20-spin counts of the F-counter, spaced 5 sec apart at the time when it pointed to the geomagnetic north near the horizon, and plotted once every precession. Also plotted are luminosities of the two emission lines, 4278 Å and 5577 Å, at the intersection of the auroral arc with the geomagnetic meridian, observed by means of the meridian-scanning photometers on the ground (FUKUNISHI and TOHMATSU, 1973), so that the same part of the auroral arc is covered both by the X-ray counter and the photometer. It is likely that the time variation of X-ray intensity is well correlated with those of luminosities overall despite the difference in their solid angles.

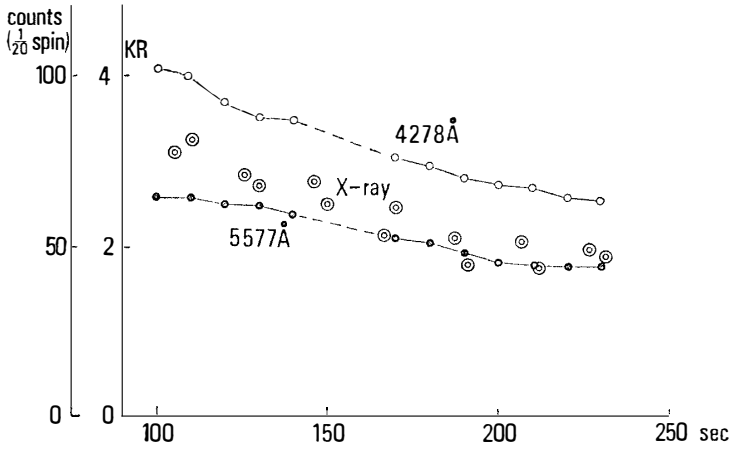

Fig. 26. Time variations of optical emission lines, 4278 Å and 5577 Å, appeared in the same direction with the line of sight of the X-ray counter at Syowa Station. The X-ray intensity is given by 1/20-spin counts taken by the forward X-ray counter every precession.

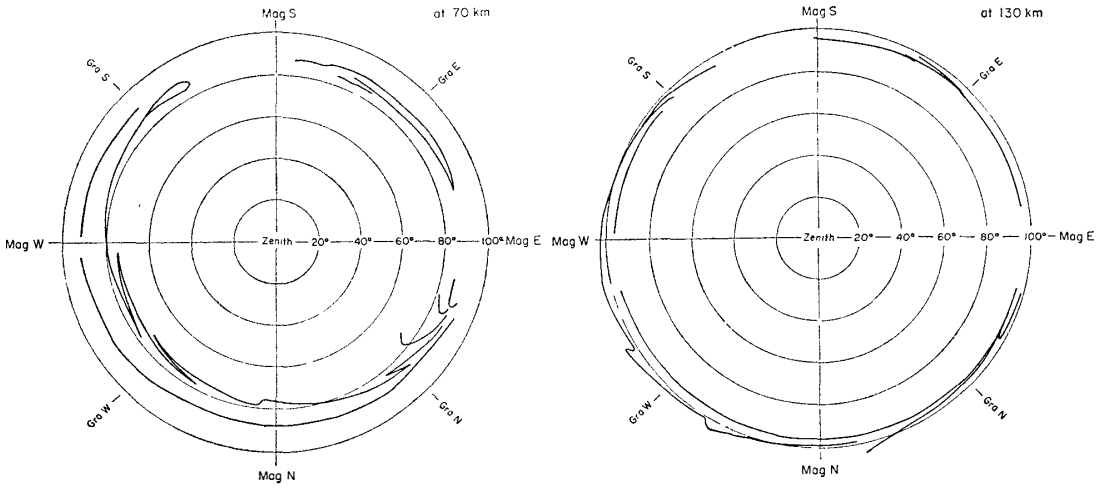

Fig. 27. Examples of spatial distributions of visual aurora viewed from rocket altitudes of 70 km and 130 km. They were transferred from the all-sky photographs of Fig. 8 by assuming the auroral altitude to be 110 km. The locations of the brightest arcs are substituted by lines.

Thus, the brightest zone of luminosities already passed away from overhead when the rocket was fired. Assuming the auroral altitude to be a certain fixed value, we can trace from the all-sky camera photographs the spatial patterns of luminosities viewed from any rocket altitude. Choosing 110 km as the auroral altitude from the results in Section 6, polar coordinate patterns of the auroral luminosities looked at from two selected altitudes, 70 km and 130 km, are shown in Fig. 27. In this case, each of the individual arcs was illustrated by an approximated contour line to distinguish them from each other. The thus derived contour lines were drawn on the sequential iso-photo maps of auroral X-rays achieved previously. Some selected examples of them are given in Fig. 28(a)-(c), where luminosity contours are indicated by dotted lines. It is evident from each diagram of Fig. 28 that the dotted lines almost pass through the zonal region in which peak X-ray fluxes were observed, regardless of the rocket altitude. It is, therefore, concluded that a certain region of the atmosphere from which auroral X-rays are emitted fairly well coincides with the region of the brightest auroral luminosity.

8.2. Riometer, geomagnetic activity and optical emissions

To see how much the degree of aurora is concerned with the present rocket experiment, related geophysical phenomena such as geomagnetism, riometer, VLF and ULF emissions and optical emission lines were examined. Fig. 29 shows time characteristics of these phenomena before and after the rocket experiment, where the geomagnetic H-component, cosmic noise absorption of 30 MHz,

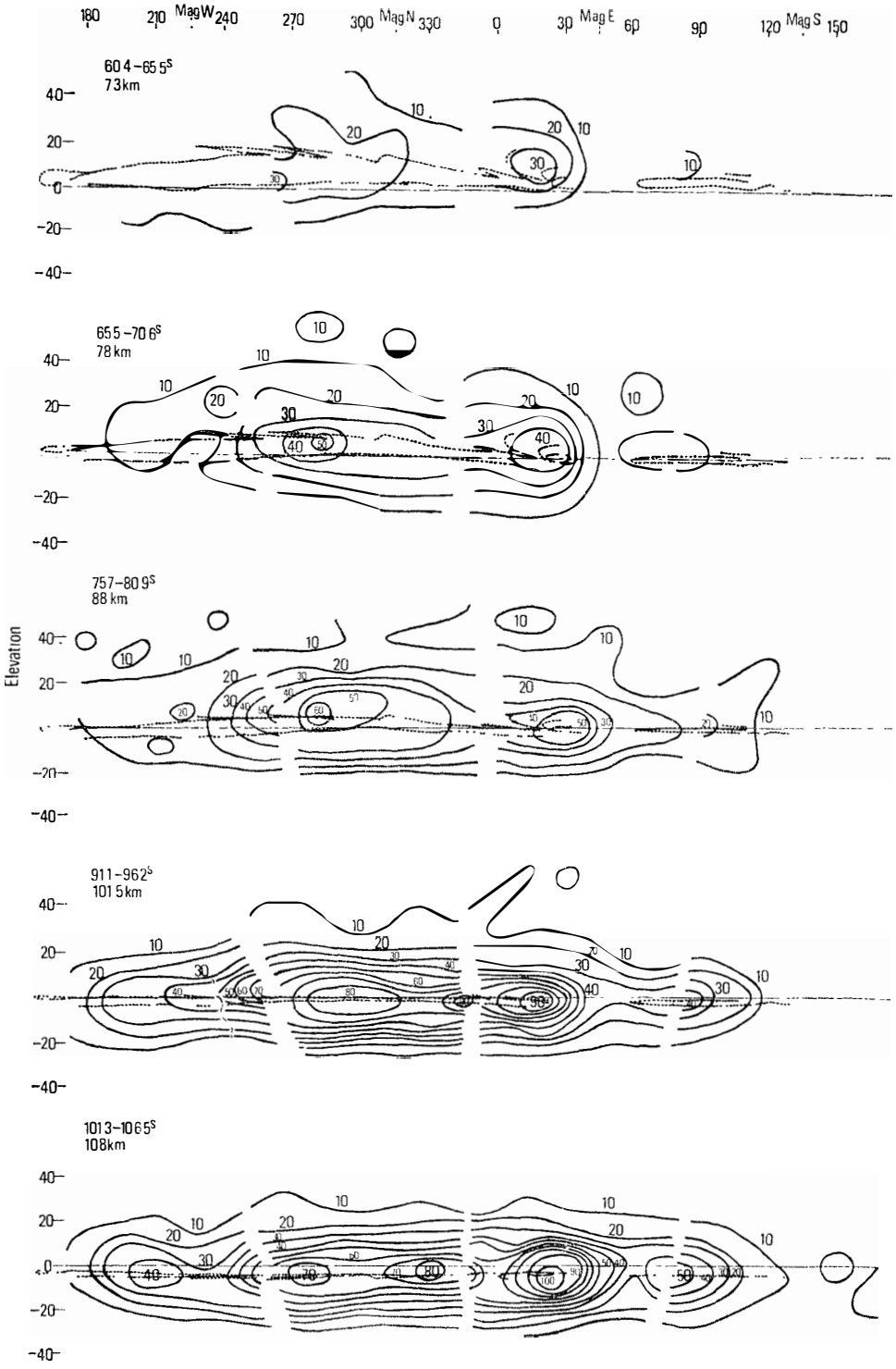

Fig. 28(a)-(c). Selected examples of iso-photo maps of auroral X-ray intensities, with dotted lines displaying the locations of the brightest arcs of visual aurora.

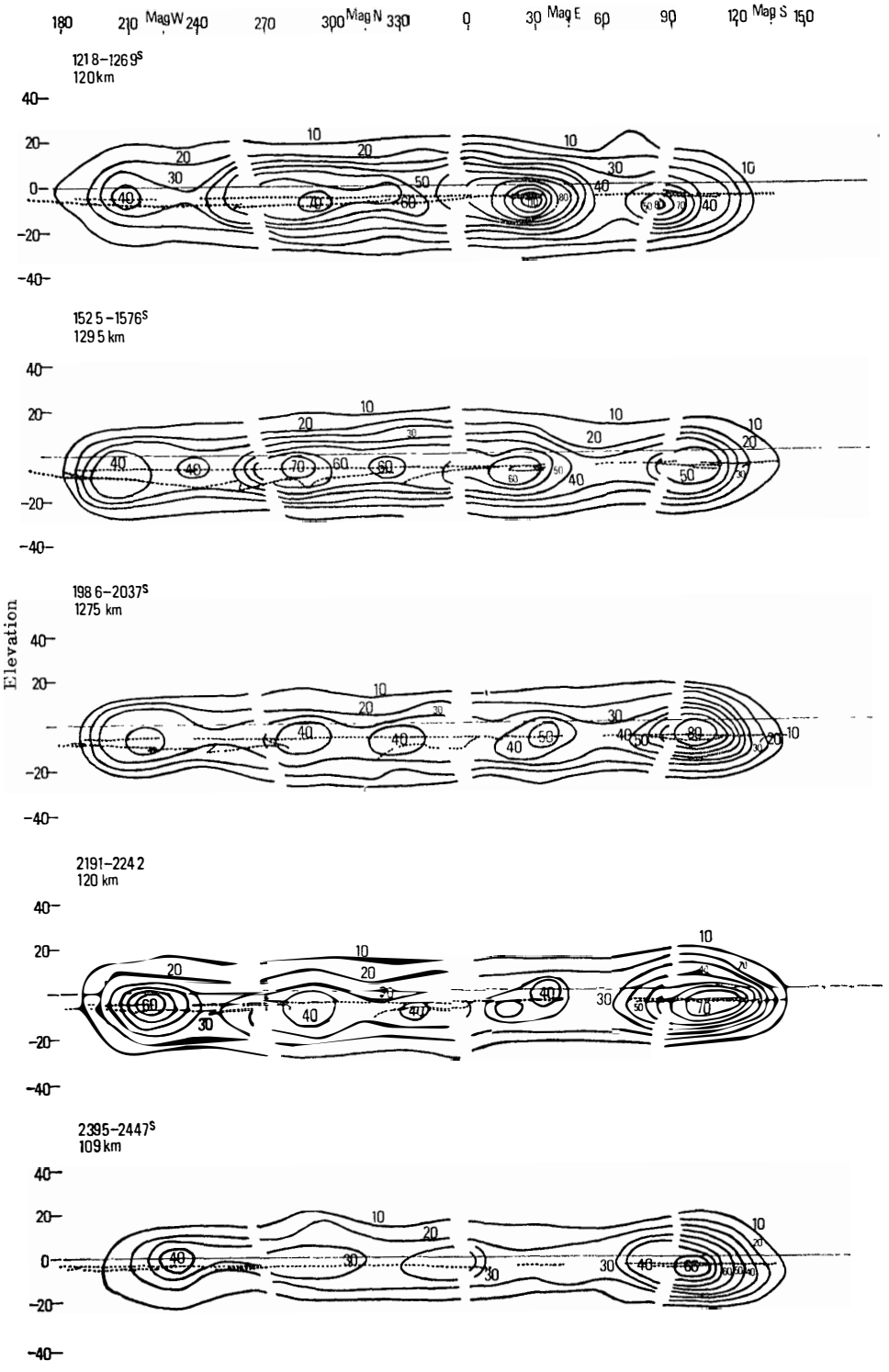
180 210 Mag W 240 270 300 Mag N 330 0 30 Mag E 60 90 120 Mag S 150
1218–1269S
120km
1525–1576S
1295 km
1986–2037S
1275 km
2191–2242
120 km
2395–2447S
109 km
Elevation
40
20
0
-20
-40

Fig. 28(b)

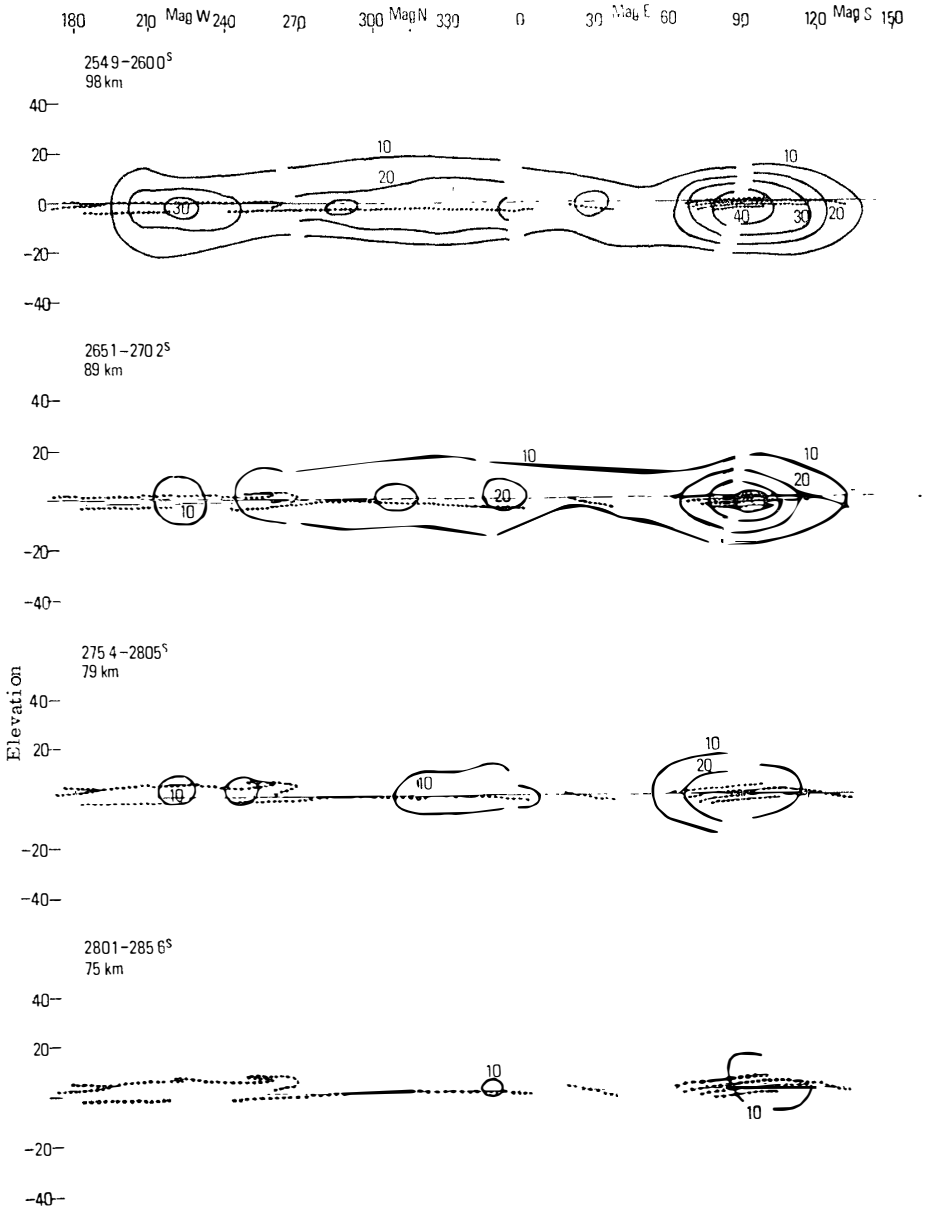

Fig. 28(c)

VLF emissions at 930 Hz and 8 kHz bands, dH/dt, 5577 Å and 6300 Å lines from Syowa Station are indicated respectively.

As seen in the figure, several auroral activations occurred over Syowa Station, but all of them were not severe. Judging from these time behaviors, it is considered that the auroral activity associated with the present rocket experiment was one of activations of a discrete arc in the pre-midnight sector which occurred during general, moderate activities throughout the night.

The rapid drift of aurora from south-east to north-west during the rocket

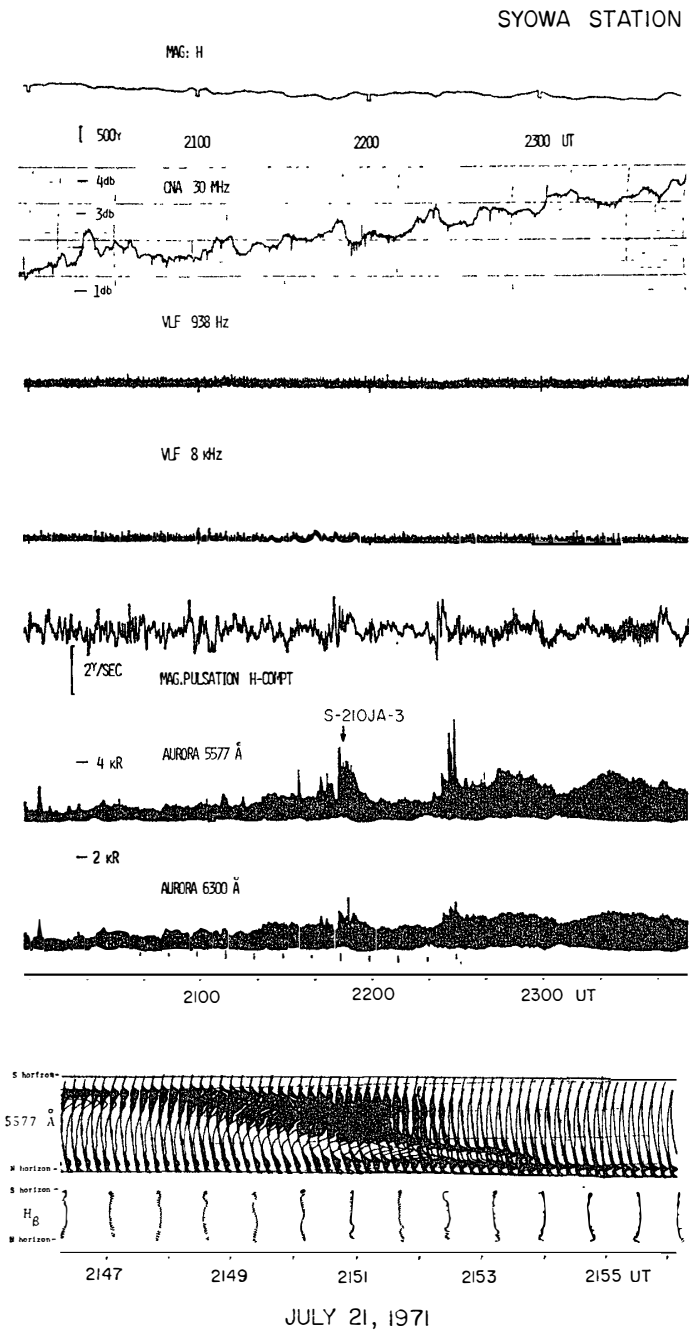

Fig. 29. Time variations of a variety of geophysical activities observed at Syowa Station before and after the rocket experiment. The bottom panel represents temporal changes in the meridian profiles of 5577 Å (upper) and H_β (lower) emissions during the rocket experiment (both in arbitrary scale). A tilting filter system was adopted for the H_β photometer so that the intensity of H_β emission is given in amplitudes of wave form.

experiment indicates that the activity over Syowa was the western end of the total activity having its center of activation a little east of Syowa Station. In other words, it was a typical westward travelling surge as seen in the bottom of Fig. 29 in the form of latitude-time displays, related to a breakup which occurred in the midnight sector. The magnetic variation during the passage of the surge over Syowa was a bay-like depression of H amounting to about -200 γ and related enhancements of VLF hiss emission were observed. Cosmic noise absorption of about 0.7 db and depression of the H_β emission were also related to the surge. TV observations of aurora were also carried out simultaneousiy. Unfortunately, however, the field of view did not cover the active aurora since it was directed towards the rocket trajectory from which the active aurora had drifted away.

8.3. Auroral X-rays in balloon altitudes

In association with this rocket flight, a number of balloon flights for auroral X-ray observations were carried out at several stations in the northern and southern hemispheres. A summary of them is illustrated in Fig. 30. The co-ordinated balloon campaign was conducted over Northern Norway and Iceland (TREFALL and BROWN, 1972), and two balloons were released from Syowa Station. The rocket was launched during the level floatings of four of 58 balloons in the former case. Unfortunately, one of those from Reykjavik, being nearly geomagnetically conjugate to Syowa Station, was released just after the rocket experiment. Also, one of the two from Syowa Station suffered telemeter fad-out only 10 minutes before the rocket launch.

As an example of simultaneous balloon flights with the rocket, Fig. 31 gives

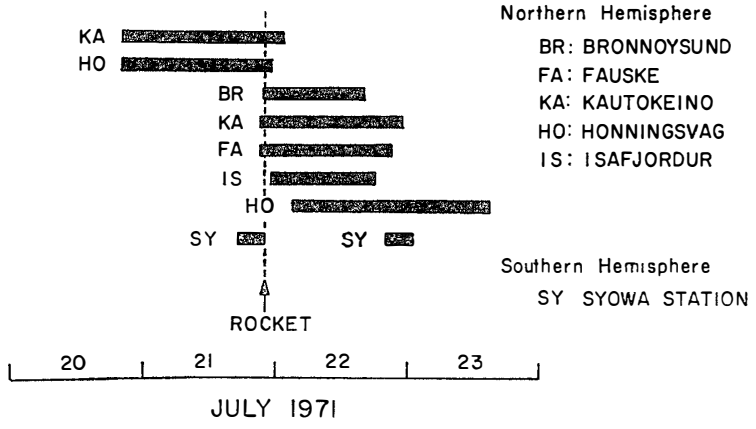

Fig. 30. The observation time of the auroral X-ray balloons launched from several stations in the northern and southern hemispheres before and after the rocket experiment.

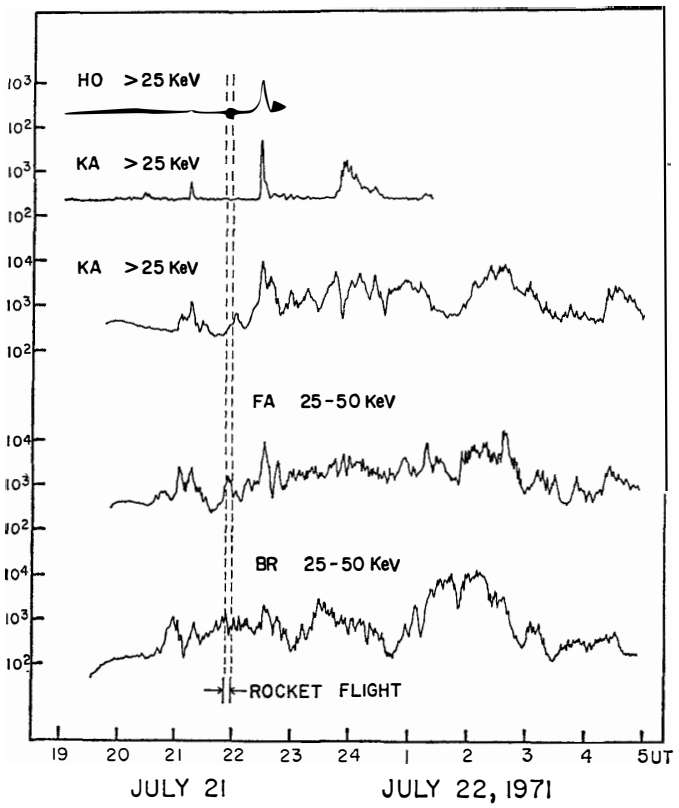

Fig. 31. Intensity-time profiles of auroral X-rays observed by means of several simultaneous balloon flights with the rocket flight. Balloon notations are identical to those given in the right-hand side of Fig. 30. The time interval of the rocket flight is indicated by double broken lines.

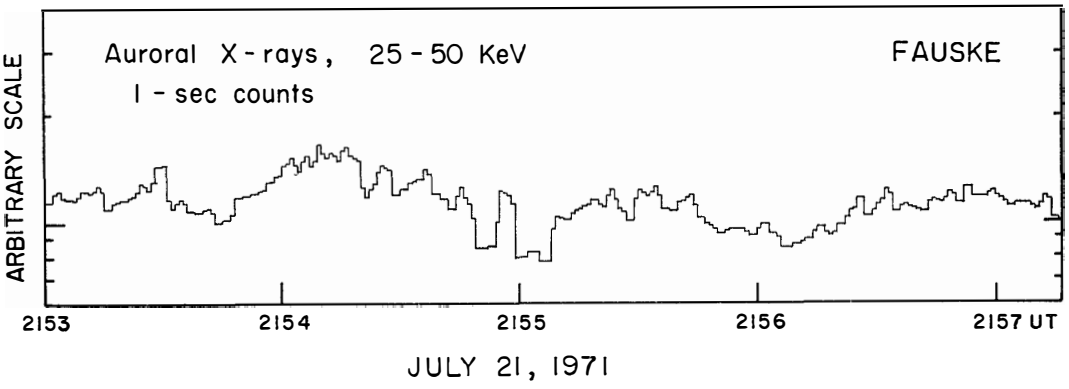

Fig. 32. Time variations of 1-sec counts of auroral X-ray intensities observed during the rocket flight by a balloon from Fauske, Norway.

the time profiles of auroral X-ray intensities observed by five balloons from the Norwegian stations. At the time of the rocket observation, there occurred an enhancement of X-rays, evident though not prominent as seen in the figure, in the area of the FA and KA balloons almost coincident with the enhancement of green line emission seen at Syowa Station (Fig. 29).

The other example of a simultaneous record with 1-sec resolution given in Fig. 32, also indicates some resemblances to the time variation of X-rays at source S1 in Fig. 21, both having broad peaks around 2154.2 and 2155.5 UT, although the intensity at S1 fluctuates more than that at the FA balloon. This suggests that the FA balloon at that time was probably located a little east of the conjugate point of Syowa Station.

The next auroral activity which occurred at 2225 UT, although being out of the period of the rocket experiment here and accordingly not directly related to the present contents, is still of interest. This auroral activity at Syowa Station is quite similar to the previous, namely not so active one, nevertheless the corresponding northern activity covers in contrast a very extended area. All balloons observed it as seen in Fig. 30, suggesting almost simultaneous auroral activation over the northern Atlantic. It may be worth noting that a great deal of geomagnetic pulsation activity and related auroral pulsation occurred in the morning following these events at Syowa Station.

9. Discussions and Conclusions

For image formings of auroral X-rays, a sounding rocket carried two identical scintillation counters to an auroral altitude of close to 110 km. The flight character of both spinning and precession motions of the rocket was utilized as much as possible for sky scannings by the counters which were mounted inclined from the spinning axis. Since, fortunately, appreciable amounts of fluxes of X-rays from a relatively active aurora were detected, we succeeded in tracing the spatial pattern of X-rays once every five seconds in virtue of an unexpectedly large precession motion.

In general, auroral X-rays at rocket altitudes or greater are associated with their parent energetic electrons. So a NaI scintillation counter unprotected for charged particles aboard a rocket used to detect both X-rays and their parent electrons, when the rocket hit the precipitating region of electrons. In this experiment, again fortunately, a smaller contribution of electrons was received, because the precipitating regions were already far from the observation point when the rocket came close to an auroral altitude. Accordingly, most of particles detected by the present counters can be identified to be photons.

In the process of making the iso-photo maps, two ambiguities were introduced by unfavorable instrumental sources. One was due to a slight difference in the detection efficiency between the two counters, forward and backward, of about 20% or so as described in Section 2. Since a sheet of the map was composed of alternative patterns from the F- and B-counters, a certain amount of discontinuities on the contour lines arose in the gaps between one pattern and the adjacent. Hence, the spacing which appeared in each pattern of Fig. 19 (also in Fig. 28) was taken from this reason.

The other ambiguity was based on the wide-angled field of view, about 20°, of the counter telescope in this experiment. Therefore, it may be said that the iso-photo maps of X-rays obtained as an image of source distribution is a kind of photograph out of focus. The spread of the maps along the elevation in Fig. 19, which is found almost always to be $\sim 40°$, is nearly equal to the apparent spread coming from the limitation of the spatial resolution of

the equipment. In other words, this suggests that the X-ray sources are really distributed on a very thin layer probably along the visual auroral arcs.

In addition, the trajectory of variable viewing directions of the X-ray counter accompanied by the spinning motion was not circular but spiral along the nose or tail locus of the rocket. Hence, the present procedure of analysis, where a train of circles was adopted for simplicity as seen in Figs. 17 and 18, includes some azimuthal ambiguities between one circle and its adjacent ones, amounting to 13.8° at maximum. In Section 5 we mentioned that 26 spinning motions were contained during a precession period. But, strictly speaking, a short time of 0.1 spin should be added throughout the eleven precessions in total. This results in a time elongation of 7.16 msec for a precession, corresponding to an angular displacement of 0.3 minutes per spin. Though such a discrepancy is negligibly small in the initial stage of the precession, it accumulates more and more with time and finally becomes an angular discrepancy of 36° between the first and the last precessions. In connection with these, a least square method fitted to all the data points would be expected for further improved studies of image formings of auroral X-rays.

The X-ray intensity along the auroral arc shows distinct inhomogenities, such as the point sources referred to in Fig. 20, and moreover each source intensity varies fairly rapidly in somewhat independent manner as seen in Fig. 21. These facts give an important physical meaning to auroral X-ray studies based on balloon observations. In most cases of the balloon observations carried out so far, the omnidirectional detector, which is usually insensitive to the position of a limited X-ray source, has widely been used for its conventional treatment. The intensity-time profiles thereby obtained are related to the very gross feature of the fluxes integrated all over the sky, such as for example, the simple average of the five curves of Fig. 21. This situation is apt to lead us to an incorrect conclusion when we compare them with those of the other associated auroral phenomena. Therefore, the necessity of a position-sensitive observation is emphasized for further studies of auroral X-rays.

Recently, OGUTI (1975) classified optical auroral phenomena into various types of formations by means of TV camera pictures and pointed out the existence of the folding type of splitting aurora. It would be interesting if the interrelation between the above-mentioned variations of X-rays and the splitting aurora were explored by simultaneous rocket and TV observations.

In conclusion, the following is a summary of this work.

1. 44 iso-photo maps of auroral X-rays displaying their spatial distributions as viewed from rocket altitudes were composed with 5-sec spacing.

2. The production layer of auroral X-rays concentrated into a very thin range of elevation and almost coincided with the region from which arise the

brightest luminosities of aurora.

3. Several localized sources of X-rays were found along the azimuth and the rapid intensity variations from them revealed different patterns of profile from source to source.

4. The azimuthal distribution of ultraviolet emissions at the auroral altitude correlated well with that of auroral X-rays overall, except for some dissimilarities in local fluctuations of X-ray fluxes.

Acknowledgments

This rocket experiment was carried out by the wintering party of the 12th Japanese Antarctic Research Expedition, which was conducted by one of the authors (OGUTI). The authors wish to thank Professor H. TREFALL for supplying us with unpublished time profiles of auroral X-ray records taken at northern hemisphere balloon stations. Also thanks are due to Dr. T. TOHMATSU for his prompt supply of ultraviolet emission data obtained from the same rocket experiment.

References

BROWN, R. R. (1966): Electron precipitation in the auroral zone. Space Sci. Rev., **5**, 311–387.

BROWN, W. L., L. J. CAHILL, L. R. DAVIS, C. E. MCILWAIN, and C. S. ROBERTS (1968): Acceleration of trapped particles during a magnetic storm on April 18, 1965. J. Geophys. Res., **73**, 153–161.

FUKUNISHI, H. and T. TOHMATSU (1973): Constitution of proton aurora and electron aurora substorms. JARE Sci. Rep., Ser. A, **11**, 1–78.

IMHOF, W. L., G. H. NAKANO, R. G. JOHNSON, and J. B. REGAN (1974): Satellite observations of bremsstrahlung from widespread energetic electron precipitation events. J. Geophys. Res., **79**, 565–574.

IMHOF, W. L. (1974): Review of rocket and satellite measurements of X-rays from electron precipitation at high altitudes. Proc. Int. Conf. 'X-Rays in Space', Calgary, **2**, 741–775.

KAMIYAMA, H. (1966): Flux of bremsstrahlung photons caused by energetic electrons precipitating into the upper atmosphere. Rep. Ionos. Space Res., **20**, 374–394.

KREMSER, G. (1973): Recent results of auroral X-ray measurements. SPARMO Bull., **6**, 183–195.

KODAMA, M., K. OGURA, E. TAMAI, and T. OGUTI (1972): Balloon observation of auroral X-rays at Syowa Station, Antarctica—Measurements for the geomagnetic conjugacy. Rep. Inst. Phys. Chem. Res., **48**, 145–165.

KODAMA, M. and T. OGUTI (1974): A rocket experiment for image formings of auroral X-rays at Syowa Station, Antarctica. Proc. Int. Conf. 'X-Rays in Space', Calgary, **2**, 1090–1094.

OGUTI, T. (1975): Metamorphoses of aurora. Mem. Natl Inst. Polar Res., Ser. A, **12**, 1–101.

PARKS, G. K. (1970): The acceleration and precipitation of Van Allen outer zone energetic electrons. J. Geophys. Res., **75**, 3802–3816.

ROBERTSON, I. W. H., D. D. WALLS, C. D. ANGER, and D. W. JOHNSON (1974): A rocket experiment for imaging the aurora by means of high speed photometric scanning. Planet. Space Sci., **22**, 1003–1015.

SELTZER, S. M., M. J. BERGER, and T. J. ROSENBERG (1973): Auroral bremsstrahlung at balloon altitudes. NASA, Sp–3081.

TOHMATSU, T., T. OGUTI, E. KANEDA, T. NAGATA, and M. KODAMA (1974): Auroral UV and X-ray emissions in Antarctica. Mem. Natl Inst. Polar Res., Special Issue, **3**, 21–28.

TREFALL, H. (1970): Balloon measurements of bremsstrahlung X-rays from electron precipitation events in the auroral zone. SPARMO Bull., **9**, 185–219.

TREFALL, H. and R. R. BROWN (1972): Report on balloon flights from northern Norway and Iceland 1971. SPARMO Bull., **5**, 17–33.

TREFALL, H. (1974): Private communication.

TREILHOU, J. P. (1974): Preliminary results of multi-balloon observations of X-rays in auroral conditions. Proc. Int. Conf. 'X-Rays in Space', Calgary, **2**, 1053–1068.

VENKATESAN, K. K. V. D. and C. D. ANGER (1975): Investigation of electron precipitation during an auroral substorm by rocket-borne detectors. J. Geophys. Res., **80**, 3205–3210.

(Manuscript received February 28, 1976)